Title
An Allosteric Anti-tryptase Antibody for the Treatment of Mast Cell-Mediated Severe Asthma

Journal
Cell, 179(2)

ISSN
0092-8674

Authors
Maun, Henry R
Jackman, Janet K
Choy, David F
et al.

Publication Date
2019-10-01

DOI
10.1016/j.cell.2019.09.009

Peer reviewed

HHS Public Access

Author manuscript

Cell. Author manuscript; available in PMC 2021 August 30.

Published in final edited form as:

Cell. 2019 October 03; 179(2): 417–431.e19. doi:10.1016/j.cell.2019.09.009.

An allosteric anti-tryptase antibody for the treatment of mast cell-mediated severe asthma

Henry R. Maun[#1], Janet K. Jackman[#2], David F. Choy[#3], Kelly M. Loyet[#4], Tracy L. Staton[#5], Guiquan Jia[3], Amy Dressen[6], Jason A. Hackney[7], Meire Bremer[5], Benjamin T. Walters[4], Rajesh Vij[8], Xiaocheng Chen[8], Neil N. Trivedi[9,18], Ashley Morando[4], Michael T. Lipari[1], Yvonne Franke[10], Xiumin Wu[11], Juan Zhang[11], John Liu[11], Ping Wu[12], Diana Chang[6], Luz D. Orozco[7], Erin Christensen[13], Manda Wong[12], Racquel Corpuz[12], Julie Q. Hang[13], Jeff Lutman[14], Siddharth Sukumaran[14], Yan Wu[8], Savita Ubhayakar[15], Xiaorong Liang[15], Lawrence B. Schwartz[16], Magda Babina[17], Prescott G. Woodruff[9], John V. Fahy[9], Rahul Ahuja[9,18], George H. Caughey[9,18], Aija Kusi[19], Mark S. Dennis[8], Charles Eigenbrot[12], Daniel Kirchhofer[1], Cary D. Austin[20], Lawren C. Wu[2], James T. Koerber[8], Wyne P. Lee[11], Brian L. Yaspan[6], Kathila R. Alatsis[19], Joseph R. Arron[2,#], Robert A. Lazarus[1,#], Tangsheng Yi[2,21,#]

[1]Department of Early Discovery Biochemistry, Genentech, Inc. 1 DNA Way, South San Francisco, CA 94080, USA.

[2]Department of Immunology Discovery, Genentech, Inc. 1 DNA Way, South San Francisco, CA 94080, USA.

[3]Department of Biomarker Discovery OMNI, Genentech, Inc. 1 DNA Way, South San Francisco, CA 94080, USA.

[4]Department of Biochemical and Cellular Pharmacology, Genentech, Inc. 1 DNA Way, South San Francisco, CA 94080, USA.

[5]Department of OMNI Biomarker Development, Genentech, Inc. 1 DNA Way, South San Francisco, CA 94080, USA.

[#]These authors are co-senior authors; address correspondence to yi.tangsheng@gene.com, lazarus.bob@gene.com, and arron.joseph@gene.com.

Author contributions

H.R.M. carried out activity assays, SEC, purified and characterized proteins and complexes for use in crystallography and helped write the paper. J.J. and K.M.L. designed and performed antibody *in vitro* and *in vivo* characterization, candidate selection, and tryptase ELISA development with A.M., M.T.L., and D.K. D.F.C. designed and analyzed human genetics and clinical response to omalizumab with A.D., D.C., L.O.G., J.A.H., and B.Y. G.J. analyzed tryptase association with asthma human biomarkers. P.W. generated crystals and C.E. solved the crystal structure. B.T.W. performed and analyzed HDX data. X.C, M.S.D., R.V., Y.W., and J.T.K. carried out antibody engineering and binding kinetics. M.T.L, D.K., E.C., M.W., R.C., and J.Q.H. established protocols and purified tryptases. Y.F. generated tryptase expression constructs. T.L.S. and K.R.A. designed and analyzed cynomolgus monkey experiment and sample analysis with M.B., J. Lutman., S.U., and X.L. N.N.T., M.B., R.A. and G.H.C. performed and analyzed tryptase activity measurements in isolated MCs in different genotypes. X.W., J.Z., J.Liu., C.D.A. and W.P.L performed humanized mouse experiments. P.G.W. and J.V.F. provided clinical asthma samples. L.B.S. and L.C.W. provided initial guidance for antibody immunization, characterization, and potential therapeutic implication for asthma. J.R.A., R.A.L. and T.Y. analyzed data and prepared the manuscript with input from all authors. J.R.A., R.A.L. and T.Y. are co-senior authors and supervised the project.

Declaration of interests

All authors except N.N.T., L.B.S., M.B., P.G.W., J.V.F., R.A., and G.H.C. are current or past employees of Genentech, Inc., a member of the Roche group, and may hold Roche stock or stock options. A patent application, entitled “anti-tryptase antibodies, compositions thereof, and uses thereof”, relating to the subject matter of this manuscript, has been filed by Genentech Inc. L.B.S. and G.H.C. are consultants for Genentech for anti-tryptase antibody development.

[6]Department of Human Genetics, Genentech, Inc. 1 DNA Way, South San Francisco, CA 94080, USA.

[7]Department of Bioinformatics, Genentech, Inc. 1 DNA Way, South San Francisco, CA 94080, USA.

[8]Department of Antibody Engineering, Genentech, Inc. 1 DNA Way, South San Francisco, CA 94080, USA.

[10]Department of Biomolecular Resources, Genentech, Inc. 1 DNA Way, South San Francisco, CA 94080, USA.

[11]Department of Translational Immunology, Genentech, Inc. 1 DNA Way, South San Francisco, CA 94080, USA.

[12]Department of Structural Biology, Genentech, Inc. 1 DNA Way, South San Francisco, CA 94080, USA.

[13]Department of Protein Chemistry, Genentech, Inc. 1 DNA Way, South San Francisco, CA 94080, USA.

[14]Department of Preclinical and Translational Pharmacokinetics, Genentech, Inc. 1 DNA Way, South San Francisco, CA 94080, USA.

[15]Department of Drug Metabolism and Pharmacokinetics, Genentech, Inc. 1 DNA Way, South San Francisco, CA 94080, USA.

[19]Department of Safety Assessment, Genentech, Inc. 1 DNA Way, South San Francisco, CA 94080, USA.

[20]Department of Pathology, Genentech, Inc. 1 DNA Way, South San Francisco, CA 94080, USA.

[9]Department of Medicine, University of California, San Francisco, San Francisco, CA 94143, USA.

[18]Veterans Affairs Medical Center, San Francisco, CA 94121, USA.

[16]Department of Internal Medicine, Division of Rheumatology, Allergy and Immunology, Virginia Commonwealth University, Richmond, VA 23298, USA.

[17]Department of Dermatology and Allergy, Charité Campus Mitte, University Medicine Berlin, Berlin, Germany.

[21]Lead contact.

[#] These authors contributed equally to this work.

Summary

Severe asthma patients with low type 2 inflammation derive less clinical benefit from therapies targeting type 2 cytokines, and represent an unmet need. We show that mast cell tryptase is elevated in severe asthma patients independent of type 2 biomarker status. Active β-tryptase allele count correlates with blood tryptase levels, and asthma patients carrying more active alleles benefit less from anti-IgE treatment. We generated a noncompetitive inhibitory antibody against human β-tryptase, which dissociates active tetramers into inactive monomers. A 2.15 Å crystal structure of a β-tryptase/antibody complex coupled with biochemical studies reveals the molecular

basis for allosteric destabilization of small and large interfaces required for tetramerization. This anti-tryptase antibody potently blocks tryptase enzymatic activity in a humanized mouse model, reducing IgE-mediated systemic anaphylaxis and inhibits airway tryptase in *Ascaris*-sensitized cynomolgus monkeys with favorable pharmacokinetics. These data provide a foundation for developing anti-tryptase as a clinical therapy for severe asthma.

Keywords

Asthma; mast cell; tryptase; anti-tryptase; allosteric protease inhibitor

Introduction

Asthma is a common human respiratory disorder characterized by episodic reversible airflow obstruction, bronchial hyperreactivity, and variable airway inflammation (Cohn et al., 2004; Maddox and Schwartz, 2002; Trivedi and Caughey, 2010). Severe asthma patients, representing 5–10% of the total asthma population, remain inadequately controlled despite intensive treatment with inhaled corticosteroids and β-adrenergic agonists, and contribute to nearly 50% of the healthcare cost of asthma (Ray et al., 2016).

Asthma is heterogeneous and driven by diverse pathogenic mechanisms (Fahy, 2015). Approximately half of asthma patients exhibit elevated markers of type 2 cytokine-driven inflammation, including blood/sputum eosinophils, fractional exhaled nitric oxide (FeNO), serum periostin, and IgE, despite similar clinical presentation to “type 2-low” patients (Fahy, 2015; Galli and Tsai, 2012; Staton et al., 2016; Woodruff et al., 2009). Antibody therapies that inhibit type 2 effector cytokines or IgE can improve lung function and reduce asthma exacerbation rates in “type 2-high” patients (Corren et al., 2011; Fahy, 2015; Hanania et al., 2013; Ortega et al., 2014; Ortega et al., 2016; Rabe et al., 2018). However, clinical studies with these agents consistently identify a subset of patients with low levels of type 2 biomarkers and limited benefit from type 2-targeted therapy, which represents a redefined unmet medical need in asthma (Corren et al., 2011; Haldar et al., 2009; Ortega et al., 2016). The molecular mechanisms driving “type 2-low” asthma are poorly understood and likely heterogeneous.

Tryptase is the most abundant secretory granule protein in human lung mast cells (MCs) (Hallgren and Pejler, 2006; Schwartz et al., 1981). It is primarily expressed in MCs and to a lesser degree in basophils (Jogie-Brahim et al., 2004). β-Tryptase, a tetrameric trypsin-like serine protease with a “donut-like” structure, is stored in human MC secretory granules in its active tetrameric form, stabilized by heparin proteoglycans (Alter et al., 1987; Hallgren et al., 2005; Schwartz and Bradford, 1986). The active site of each protomer faces the interior of the central pore, which restricts accessibility of biological substrates and inhibitors, and imposes challenges for the design of pharmacological inhibitors (Pereira et al., 1998; Sommerhoff et al., 1999). There are no known endogenous active-site inhibitors of human tryptase (Alter et al., 1990). Rather, after degranulation, tetrameric tryptase dissociates over time into inactive monomers as its natural mechanism of inactivation.

Tryptase-positive MCs are elevated in human asthmatic bronchial tissue, where they localize to epithelium, glandular, and bronchial smooth muscle regions, and their numbers correlate with airway hyperreactivity (Brightling et al., 2002; Kaur et al., 2010). Tryptase has broad biological activities, including promoting proliferation and contraction of lung smooth muscle cells (SMC), stimulating collagen production by lung fibroblasts and degrading muscle relaxing neuropeptides (Berger et al., 2001; Cairns and Walls, 1997; Franconi et al., 1989; Hallgren and Pejler, 2006; Iddamalgoda et al., 2008; Sekizawa et al., 1989; Woodman et al., 2008). Tryptase-knockout mice exhibited reduced airway hyperreactivity in an allergen-induced asthma model (Cui et al., 2014). Multiple efforts were devoted to develop oral or inhaled tryptase small molecule inhibitors (SMIs) targeting its active site (Krishna et al., 2001; Sutton et al., 2002; Wright et al., 1999). These SMIs reduced bronchial constriction and improved methacholine induced airway hyperreactivity in animal models of asthma and one ameliorated the late asthmatic response in a human Phase II allergen challenge study (Krishna et al., 2001; Sutton et al., 2002; Wright et al., 1999). However, none are currently under development due to inadequate specificity, potency, oral bioavailability, or tolerability. Development of a specific tryptase inhibitor with desired *in vivo* properties remains a challenge.

Here, we show that tryptase levels in blood and airway fluid are elevated in asthma patients and that tryptase levels in human asthmatic bronchial alveolar lavage (BAL) fluid correlate with disease severity. Elevated levels of tryptase in moderate-severe asthma are uncoupled from type 2 biomarker levels. Active tryptase degranulates MCs and active tryptase allele count in asthma patients correlates with peripheral blood tryptase levels. We generated a humanized antibody that binds to human α- and β-tryptases and potently inhibits active β-tryptases *in vitro* and *in vivo*. Our study provides a clinical rationale for developing an anti-tryptase antibody as a therapeutic agent for severe asthma, particularly for type 2 inflammation-independent subsets.

Results

Tryptase is elevated in human asthma patients independent of type 2 inflammation

To examine tryptase levels in asthma, we developed an immunoassay using two monoclonal antibodies with non-overlapping epitopes that recognize all 4 isoforms of tryptase, including α-, βI-, βII-, and βIII-tryptase monomers and tetramers (Figure S1A). We analyzed patients with different asthma severities as previously defined by their asthma symptoms and responsiveness to inhaled steroids (Jia et al., 2012; Simpson et al., 2014) and found elevated tryptase levels in BAL fluid in asthma patients compared to healthy volunteers (Figure 1A). Increased levels of tryptase in BAL fluid correlated to asthma severity with severe asthma patients exhibiting the highest levels (Figure 1A). While there were no differences in plasma tryptase levels between healthy volunteers and mild-to-moderate asthma patients, levels were significantly elevated in severe asthma patients (Figure 1B).

To understand whether type 2 inflammation is related to tryptase levels in asthma patients, we analyzed the concentration of tryptase relative to levels of type 2 biomarkers. While BAL fluid tryptase levels correlated positively with blood eosinophils and serum periostin in patients with mild asthma (Figure 1C and Figure S1B, C), this relationship was absent

in patients with severe asthma, in whom plasma and BAL fluid tryptase levels were comparably elevated in eosinophil-low and eosinophil-high subsets compared to healthy subjects (Figure 1D, E and Figure S1D–F). Taken together, these observations show that tryptase levels in asthma: 1) are elevated in airways, 2) increase with disease severity, and 3) do not correlate with biomarkers of type 2 inflammation in severe asthma.

Active β-tryptase allele count is correlated with peripheral tryptase levels

Soluble active human tryptases are produced by 2 closely spaced genes on chromosome 16: *TPSAB1* and *TPSB2*. *TPSAB1* and *TPSB2* are polymorphic and can generate 4 different isoforms: α-, βI-, βII-, and βIII-tryptase (depicted in Figure 2A) (Pallaoro et al., 1999) with α-tryptase being catalytically inactive (Huang et al., 1999). About 23% of European ancestry subjects carry a βIII-tryptase with a frameshift polymorphism (βIII^{FS}) that leads to a C-terminal tail truncation (Trivedi and Caughey, 2010). Tetramers of α- and βIII^{FS}-tryptase should lack catalytic activity (Trivedi and Caughey, 2010). Therefore, as there are 2 genes encoding active tryptase on each of 2 chromosomes 16 per subject, a given subject theoretically carries between 0–4 active β-tryptase alleles. We sequenced DNA from 473 severe asthma patients and 1,511 healthy controls of European ancestry using PCR-based Sanger sequencing to quantify active tryptase alleles spanning *TPSAB1 and TPSAB2* (total number of βI-, βII-, or βIII-tryptases). We also used whole genome next-generation sequencing (WGS) methods (Lyons et al., 2018; Lyons et al., 2016); results between Sanger sequencing and WGS are in accord (Figure S2A–C). The distributions of active tryptase allele counts were comparable between severe asthma patients and healthy controls (Figure 2B).

Next, we determined that tryptase active allele counts correspond to tryptase catalytic activity in MC lysates (Figure 2C), and active tryptase allele count strongly correlated with plasma and serum tryptase levels in healthy subjects and 2 independent asthma cohorts. Asthma patients and healthy volunteers carrying 4 active tryptase alleles have ca. 2.5-fold higher tryptase levels compared to those carrying 2 active tryptase alleles (Figure 2D–F). Genetic linkage association and WGS data revealed a small percentage of patients with increased *TPSAB1* α-tryptase copy numbers leading to increased total tryptase levels in serum and to a multisystem disorder (Lyons et al., 2016). We identified ca. 3% of patients with increased α-tryptase copy numbers who exhibited increased serum tryptase levels (Figure S2D). However, given the substantially higher proportion of patients with variation in active β-tryptase allele count, the latter is a more broadly applicable genetic modifier of systemic blood tryptase levels across the severe asthma population (Figure S2D).

We next sought to understand how active tryptase allele counts affect systemic tryptase levels. The tryptase ELISA measures all isoforms including α-tryptase (Figure S1A and Figure S2A). *In vitro*-derived MCs from subjects with 2 or 4 active alleles show similar levels of total tryptase in cell lysates (Figure S2E, F). However, as tryptase active allele counts correspond to tryptase catalytic activity in MC lysates (Figure 2C), we hypothesized that active tryptase can trigger MC degranulation in an autocrine manner, leading to augmented extracellular tryptase release. Tryptase-dependent degranulation determined by histamine release (He et al., 2004) is blocked by a selective inhibitory anti-tryptase antibody

(see below) and is also dependent on its enzymatic activity, since a catalytically inactive tryptase mutant (S195A; chymotrypsinogen numbering used throughout) has no effect (Figure 2G and Figure S2G). Recombinant β-tryptase and IgE crosslinking each has an additive effect in augmenting MC degranulation (Figure S2G–I). Tryptase inhibition with an active site SMI (Sutton et al., 2002) or 2 different inhibitory anti-tryptase antibodies reduced IgE induced MC degranulation by ca. 50% (Figure 2H). Overall, these data suggest that active tryptase allele count regulates serum tryptase levels and the amount of active tryptase stored in secretory granules, which may contribute in an autocrine manner *in vivo* to the magnitude of MC degranulation.

Active β-tryptase allele count is inversely related to clinical benefit from omalizumab treatment

Omalizumab is an IgG antibody against IgE that blocks IgE binding to FcεRI, reducing free IgE, surface FcεRI levels, and allergen-dependent MC degranulation. In clinical studies, omalizumab significantly reduces asthma exacerbations, improves asthma symptoms and quality of life, and reduces daily rescue medication use (Hanania et al., 2011). In addition, omalizumab confers modest population-wide improvement in lung function in unselected asthma patients as measured by forced expiratory volume in one second (FEV_1) (Paganin et al., 2017). To assess the relative contribution of FcεRI dependent vs. independent contributions of MCs to the clinical efficacy of omalizumab, we performed a *post hoc* analysis of a randomized placebo-controlled omalizumab Phase IIIb study (NCT00314574) to assess whether active tryptase allele count may influence the magnitude of clinical benefit. As cases or controls having 1 or 4 active tryptase alleles are relatively rare and the proportion of subjects having 2 or 3 active alleles are comparable, we dichotomized our study population as having 1 or 2 versus 3 or 4 active alleles. The baseline characteristics of these sub-groups were comparable with no statistically significant differences in demographic, clinical, or biomarker levels including serum IgE (Table S1). The subgroup having 1 or 2 active tryptase alleles exhibited statistically significant placebo-adjusted improvements for 1) mean change in FEV_1% predicted (Figure 3A left; 5.4(1, 9.9)%, $P = 0.013$), 2) mean reduction in short acting β-agonist use (Figure 3B left; −0.8(−1.5,0) puffs, $P = 0.049$), mean reduction in Total Asthma Symptom Score (TASS) (Figure 3C left; −0.7(−1.3,−0.1), $P = 0.021$), and 4) mean improvement in the Standardized Asthma Quality of Life Questionnaire (Figure 3D left, 0.5(0.1, 1), $P = 0.022$). These data suggest that higher active tryptase allele count may contribute to MC-dependent but IgE-independent clinical manifestations in asthma patients.

Generation of a humanized anti-tryptase antibody with potent inhibitory activity

We hypothesized that an inhibitory antibody against human β-tryptase could provide therapeutic benefit. Therefore, we immunized mice, rats, and rabbits with recombinant human monomeric and tetrameric βI-tryptase, panned with a human antibody phage library, and selected antibodies that bound tetramers and had >90% inhibition of βI-tryptase activity in a chromogenic peptide substrate assay. Only 9 clones with unique complementarity-determining region sequences from immunizations and one from phage were fully inhibitory (Table S2). From these, we selected 31A as the top clone for further humanization and characterization based on 1) its ability to inhibit human βI-, βII-, βIII-tryptase, 2) cross-

reactivity against cynomolgus monkey tryptase to enable preclinical pharmacokinetic (PK) and safety studies, and 3) inhibition of β-tryptase in both fragment antigen-binding (Fab) and IgG formats. Fifteen humanized variants of 31A were generated on a human IgG4 backbone and 31A.v11 was identified as the most potent antibody, having improvements of ca. 10-fold in binding affinity (K_d) and over 30-fold in inhibitory activity (IC_{50}) over the parental 31A clone (Table S3). Here, unless otherwise specified, we refer to the humanized 31A.v11 IgG4 clone as “anti-tryptase”.

Anti-tryptase inhibits tryptase catalytic activity in biochemical and cellular assays

Anti-tryptase binds to human α-, βI-, βII-, βIII- tryptase isoforms with comparable sub-nanomolar affinities (Figure 4A). Anti-tryptase also potently and completely inhibits the catalytic activity of βI-, βII-, and βIII- tryptases with comparable IC_{50} values of 4.0, 1.8, and 3.5 nM (Figure 4B); further kinetic analysis shows that anti-tryptase is a noncompetitive inhibitor (Figure S3A). Using βI-tryptase, we observed that monovalent Fab was also a complete inhibitor (IC_{50} = 3.9 nM for Fab and 1.4 nM for IgG) (Figure 4C). To see whether inhibition was simply due to a shift in pH optimum or a change in substrate specificity, we determined βI-tryptase activity at physiological heparin levels (ca. 1 μg/mL) and found that anti-tryptase was also a potent and complete inhibitor at pH 7.0 and 8.0 (Figure S3B). However, there was a small amount of residual activity at pH 6.0 from monomers that was inhibited by aprotinin (Figure S3B), in accord with previous data (Fajardo and Pejler, 2003, Fukuoka and Schwartz, 2004; Fukuoka and Schwartz, 2007). However monomers are ca. 50-fold less active than tetramers at neutral pH and strongly dependent upon heparin (Maun et al., 2018) and rapidly inactivated by protease inhibitors (Fukuoka and Schwartz, 2004), thus thought not to be physiologically relevant. We saw no change in substrate specificity in the presence of anti-tryptase upon variation in P1, P2 and P3 residues of peptide substrates (Table S4) or when using either a fluorescence-quenched peptide or Bodipy dye-labelled casein as substrates (data not shown).

Anti-tryptase also inhibits endogenous tryptase activity derived from supernatants of degranulated human MCs (Figure 4D). Vasoactive intestinal peptide (VIP) and fibrinogen have been reported as endogenous tryptase substrates (Schwartz et al., 1985; Tam and Caughey, 1990); degradation of VIP by βI-tryptase (recombinant and MC-derived) is inhibited by anti-tryptase (Figure 4E, F). Fibrinogen degradation (Ren et al., 1997) is also inhibited by anti-tryptase at pH 6.0 and 7.5 (Figure 4G).

Tryptase induces proliferation and contraction of bronchial SMC, and collagen secretion by human lung fibroblasts (Berger et al., 2001; Cairns and Walls, 1997; Woodman et al., 2008). Proliferation and contraction of SMC are dependent on catalytic activity since the S195A tryptase mutant shows no cellular effects (Figure S3C–E). Importantly, anti-tryptase inhibits all of these tryptase-dependent cellular responses (Figure 4H–J and Figure S3D). Taken together, our data show that anti-tryptase potently inhibits MC degranulation and human β-tryptase catalytic activity.

A crystal structure reveals an allosteric mode of binding and a tetramer dissociation mechanism

We hypothesized that anti-tryptase binding to active β-tryptase tetramer might result in dissociation to catalytically inactive monomers (Alter et al., 1987; Fukuoka and Schwartz, 2006; Schwartz and Bradford, 1986; Schwartz et al., 1990). Size exclusion chromatography (SEC) and SDS-PAGE analysis of tetrameric βI-tryptase with excess Fab indeed showed a ca. 80 kDa complex comprising β-tryptase monomer and Fab (Peak 3), smaller than the ca.120 kDa βI-tryptase tetramer (Peak 1) (Figure 5A, B). In the presence of heparin, a slightly larger complex (Peak 2) was observed for the βI-tryptase monomer•Fab complex (Figure 5A, B). Thus, even in the presence of heparin, which stabilizes the tetramer (Alter et al., 1987; Schwartz and Bradford, 1986), anti-tryptase Fab dissociates βI-tryptase into monomers.

To identify potential residues of the antibody binding epitope, we measured hydrogen-deuterium exchange (HDX) for monomeric βI-tryptase bound to anti-tryptase Fab over time by mass spectrometry. A local cluster of surface residues (D60e, L61, Q66, L67, L83-I88, L108-E110, shown in green) had amide bonds in slower exchange upon Fab binding, suggestive of a binding epitope, whereas other residues (S25-W29, H40, F41, H57-V59 and V231-Y233, shown in slate) were more distant from each other (Figure 5C). We sought a structure of the βI-tryptase•Fab complex, but were unable to generate crystals. Since the HDX residue cluster is distal from the active site and anti-tryptase is a noncompetitive inhibitor, we thought an active site binder might act as a crystallization chaperone. Indeed, we could generate a stable ternary complex with soybean trypsin inhibitor (STI), as shown by SEC (Peak 1) and SDS PAGE (Figure S4A, B), which crystallized and led to a 2.15 Å resolution crystal structure (Figure 5D and Table S4). βI-Tryptase residues V60c-A63, R65, P84-R87 and E109-P111 are in intimate contact (within 4 Å) with the Fab, consistent with the binding epitope suggested by HDX. The βI-tryptase•Fab contact area excludes 760 $Å^2$ from solvent (each side), with equal contributions from the Fab light chain (LC) (V30-Y32, Y34, R50, Y90, H92-Y94) and heavy chain (HC) (F50, S52-T56, Y58, R95, Y97, D98) (Figure S4C, D). Importantly, STI does not contact the Fab, justifying it as a chaperone; it only contacts βI-tryptase, excluding 1260 $Å^2$ from solvent.

When βI-tryptase monomers of the ternary complex were superposed onto tryptase protomers A and C in the WT tetramer (Pereira et al., 1998; Sommerhoff et al., 1999), the position of the corresponding Fabs are on the same side of and nearly perpendicular to the tetramer plane (Figure 5E). Most importantly, the Fab LCs would have substantial steric clashes with each other, thus preventing antibody binding to all 4 protomers while in the tetrameric state. Only tetramer dissociation would allow all the protomers to bind excess anti-tryptase Fab or IgG.

The βI-tryptase monomer•Fab complex structure revealed a significant conformational change of V60c when compared to its position in the tetramer. This would result in a steric clash with Y173d from the neighboring protomer in the large interface, which sits in a hydrophobic pocket created by residues V59, V60c, I88 and V90 (Figure 5F) in the tetramer (Maun et al., 2018; Pereira et al., 1998). We also observed Cα changes between 1–2 Å at H36, G37, P37a and Y37b in the 30s loop compared to the tetramer (Figure

5G), where Y37b is a key contact residue within 3.5 Å of its neighboring protomer in the small interface. In addition, HDX experiments indicated Fab-induced structural changes at 2 nearby residues, H40 and F41, located on the descending beta strand. To confirm that the observed structural changes in tryptase upon Fab binding lead to destabilization of both tetramer interfaces, we used βI-tryptase tetramer mutants comprising dimers that were disulfide-locked at the small or the large interface (Maun et al., 2018). Based on SEC and SDS-PAGE data, anti-tryptase Fab efficiently dissociated both types of tetramers into dimers, thus capable of destabilizing both the small and large interfaces (Figure 5H, I). Due to a 2-fold axis in the tetramer, each interaction exists twice, thus enhancing destabilization. Taken together, the biochemical and structural data show that anti-tryptase binds and inhibits β-tryptase by a unique allosteric mechanism, distinct from active site SMIs, which do not dissociate the active β-tryptase tetramer.

Anti-tryptase inhibits tryptase activity *in vivo* and attenuates MC-induced anaphylaxis responses

We next sought to determine whether anti-tryptase could inhibit tryptase biological activity *in vivo*. Since the antibody binds human and cynomolgus monkey, but not rodent tryptases, we utilized a NOD.*scid* IL2rg^{null}SCF/GM-CSF/IL-3 (NSG-SGM3) mouse model with human MC engraftment as previously reported (Bryce et al., 2016). Eight weeks after human stem cell transplantation, we validated human MC engraftment in spleen and lung (Figure 6A). Engrafted MCs expressed surface hFcεRI, hKIT (CD117) and intracellular tryptase (Figure 6A, B), and we detected human tryptase in the engrafted mouse serum (Figure 6C). Tryptase induces microvascular leakage during the anaphylaxis reaction (He and Walls, 1997). To induce MC degranulation and tryptase release, we injected animals with an anti-NP human IgE and subsequently crosslinked IgE with NP-BSA conjugates *in vivo*, which induced a 7-fold increase in serum and active lung tryptase (Figure 6C). Anti-tryptase treatment significantly reduced the IgE-induced systemic anaphylaxis response (Figure 6D). To quantify the amount of active tetrameric tryptase in tissues and whether our antibody inhibits tryptase in lungs, we generated a biotinylated activity-based probe (ABP) (Pan et al., 2006) that covalently binds at the active site and used a non-interfering anti-tryptase antibody for active tryptase capture and detection (Figure S5 A–D). Upon NP-IgE crosslinking, significantly elevated active tryptase levels were detected in BAL fluid, which is completely blocked by anti-tryptase (Figure 6E) and we observed significantly reduced tryptase catalytic activity in the BAL fluid (Figure 6F). Taken together, our antibody potently inhibits active tryptase *in vivo* and attenuates IgE-induced systemic anaphylaxis responses.

Anti-tryptase exhibits favorable pharmacokinetics and reduces tryptase activity in BAL fluid in nonhuman primates

To investigate the PK properties and partitioning to lung tissue of anti-tryptase antibody, we dosed NOD.*scid* mice and cynomolgus monkeys with anti-tryptase IgG4 and observed low systemic clearance, similar to an anti-gD control antibody (Figure 7A, B). The half-life of anti-tryptase in cynomolgus monkeys was ca. 15 days (Figure 7B).

We also assessed anti-tryptase exposure in BAL fluid as a proxy for lung tissue. Antibody levels in BAL fluid were ca. 20% of blood levels (Figure 7C). Slightly higher levels of antibody in BAL were observed for anti-tryptase compared to anti-gD isotype control, which could be driven by a target mediated retention effect. BAL active tryptase levels in cynomolgus monkey were measured using an ABP immunoassay (Figure S5). Two out of three cynomolgus monkeys had detectable baseline activity in BAL fluid. After anti-tryptase treatment, BAL tryptase activity was largely undetectable for over 2 weeks (Figure 7D). We assessed a cohort of cynomolgus monkeys that were sensitized to *Ascaris suum* (*A. suum*) and had elevated active tryptase levels in BAL fluid after inhaled *A. suum* challenge. After sensitization was complete, these animals underwent a vehicle phase and drug phase, receiving an inhaled *A. suum* challenge prior to BAL fluid collection during each phase (Figure 7E). Treatment with anti-tryptase antibody significantly reduced BAL active tryptase levels and urine histamine metabolites (Figure 7F and Figure S6), leading to undetectable BAL tryptase activity in 4 of 5 animals with detectable BAL tryptase activity in the vehicle phase. In animals with highest levels of BAL tryptase activity in vehicle phase, BAL active tryptase levels were reduced by greater than 90% after treatment with anti-tryptase in the drug phase. In summary, these data show that systemically administered anti-tryptase sustainably inhibits tryptase activity in lungs of mice and nonhuman primates.

Discussion

Asthma is a chronic obstructive respiratory disorder with episodic reversible airflow obstruction and variable inflammation (Cohn et al., 2004; Fahy, 2015). Although the underlying mechanisms are unclear, type 2 inflammation-independent asthma represents a significant unmet medical need (Fahy, 2015). Here, we show that MC tryptase levels in serum and BAL fluid correlate with asthma severity and tryptase is elevated in airways of severe asthma patients independent of type 2 biomarker levels. Genetic variation at the tryptase locus results in different numbers of active tryptase alleles. Active tryptase allele count is correlated with tryptase levels and moderate-severe asthma patients carrying greater numbers of active tryptase alleles exhibited attenuated clinical benefit from anti-IgE therapy. These observations suggest that neutralization of tryptase activity is a promising therapeutic strategy for type 2-independent asthma, which is resistant to currently available asthma therapies.

Accumulating data indicate that MCs are critical mediators of airway obstruction and hyperreactivity (Berry et al., 2007; Brightling et al., 2002; Kaur et al., 2010; Siddiqui et al., 2018). As a major MC granule protein (ca. 25% of cell protein) (Schwartz et al., 1981), tryptase levels are elevated in BAL fluid and correlated with type 2 biomarkers in mild asthma patients, consistent with observations that intraepithelial MC numbers are greater in type 2-high mild asthma (Dougherty et al., 2010). However, we observe that tryptase is further elevated in BAL fluid in moderate-severe asthma patients independent of type 2 biomarker levels. The difference between mild and moderate-severe asthma patients may result from different MC recruitment mechanisms in various disease stages and/or the effects of inhaled glucocorticoid therapy in moderate to severe asthma. In mild asthma patients, type 2 cytokines such as IL-33, TSLP, IL-4, IL-5, and IL-13 may contribute to MC recruitment to the bronchial epithelium (Bradding and Brightling, 2007).

However, severe asthma patients often have more extensive tissue remodeling with smooth muscle layer expansion and tissue fibrosis, which may provide a niche for MCs. Airway SMC and fibroblasts can produce chemotactic factors for MC recruitment, which may be independent of type 2 inflammation (El-Shazly et al., 2006; Page et al., 2001; Sutcliffe et al., 2006). Tryptase is a major MC product with pleiotropic biological activities in promoting SMC proliferation, fibroblast collagen secretion, and tissue extracellular matrix protein degradation, all of which may contribute to chronic tissue remodeling (Page et al., 2001). Further mechanistic research is needed to fully understand the interplay between airway SMC, MCs and type 2 independent MC recruitment mechanisms. Ongoing clinical studies of anti-tryptase in asthma may reveal further roles of tryptase in asthma symptoms and tissue remodeling.

Soluble human catalytically active tryptases are encoded by 2 closely spaced genes, *TPSAB1* and *TPSB2*. *TPSAB1* comprises 2 principal alleles that encode α- and βI-tryptases whereas *TPSB2* alleles principally encode βII-, βIII-tryptases. High sequence similarity of tryptase isoforms and haplotype structure at the tryptase loci preclude simple SNP-based genotyping or the use of antibodies to distinguish tryptase isoform composition in individual subjects. Recently, genetic linkage association and WGS data revealed a small percentage of patients with α-tryptase copy number variation; duplication or triplication of α-tryptase leads to hereditary α-tryptasemia with increased total tryptase in serum and multisystem disorders (Lyons et al., 2016). These patients have increased frequency of gastroesophageal reflux symptoms, vibration induced urticaria, and flushing/pruritus. While α-tryptase is catalytically inactive, a very recent study has shown that α/β-tryptase heterotetramers are active, having altered substrate specificities from β-tryptase homotetramers, and capable of cleaving EMR2 and inducing vibration-triggered mast cell degranulation and urticaria (Le et al., 2019). Our antibody should inhibit α/β-tryptase heterotetramers as it binds α- and β-isoforms with comparable subnanomlar affinities (Figure 4A), thus it may also have relevance in hereditary α-tryptasemia related disorders. The likelihood that additional substrate preference differences between β-tryptase homotetramers and α/β-tryptase heterotetramers or heterotetramers with different α/β-tryptase ratios may exist suggests additional levels of regulation of tryptase biological activity in various physiological situations.

Asthma patients with increased active tryptase allele counts have higher levels of blood tryptase. Active tryptase alleles determine the amount of tryptase activity in MC lysates, but do not affect tryptase mRNA transcript nor total tryptase granule protein. Tryptase catalytic activity is critical for triggering MC degranulation in a feed-forward manner; tryptase release may be “piecemeal” in the absence of a strong degranulation stimulus (Dvorak et al., 1992; Gaudenzio et al., 2016), which may explain the relationship between active tryptase allele count, tryptase release from MCs, and systemic tryptase levels. Consistent with this scenario, patients with higher active tryptase allele count had attenuated anti-IgE treatment responses, suggesting that for those with high β-tryptase, blockade of IgE/FcεRI interactions are insufficient to stabilize MCs. While tryptase genetics contribute to clinical responses to omalizumab, β-tryptase allele distributions do not differ between controls and asthma patients. Therefore, tryptase is more likely a modifier of asthma phenotypes than a risk factor for incident asthma. This situation is analogous to how asthma patients with elevated

blood eosinophil counts respond better to anti-IL5 treatment than those with lower blood eosinophil counts despite having similar disease severity at baseline: eosinophils modify the asthma phenotype in a subset of patients and those patients are more likely to benefit from eosinophil-targeting therapies (Fahy, 2015). Our study is a post-hoc analysis from a single phase III trial that was not designed to test how genetics affect disease manifestations. With an increased understanding of tryptase genetics (Lyons et al., 2016; Trivedi et al., 2009), future studies with larger cohorts across diverse genetic backgrounds are needed to assess how active tryptase allele counts, α/β tryptase ratio, and α-tryptase copy number variation may contribute to asthma pathogenesis; it will also be of interest to assess tryptase genetics in the context of clinical responses to other asthma therapies beyond omalizumab.

To generate a tryptase inhibitor with drug-like potency, selectivity, and PK, we conducted an extensive antibody campaign, identified 10 inhibitory anti-tryptase antibodies, and humanized one for further characterization. This antibody potently inhibits tetrameric β-tryptase in biochemical and cell-based assays by dissociating the active β-tryptase tetramer into inactive monomers. Similar tetramer dissociation phenomena have been described for a previously described nonhuman anti-tryptase antibody and lactoferrin (Fukuoka and Schwartz, 2006; Hallgren et al., 2001). Heparin stabilizes the active tryptase tetramer; after secretion, the lower extracellular heparin concentrations result in the subsequent dissociation into inactive monomers as a natural mechanism of inactivation (Hallgren et al., 2001; Schwartz et al., 1990). Therefore, while it is possible that anti-tryptase simply promotes tetramer dissociation by displacing heparin, similar to the mechanism of lactoferrin (Elrod et al., 1997; Hallgren et al., 2001), this is not the case, since heparin still binds to the Fab•βI-tryptase complex (Figure 5A, B). Ultimately, the crystal structure of the Fab•tryptase complex and biochemical data revealed that the Fab binds to an unexpected exosite, allosterically and noncompetitively inhibiting enzymatic activity by destabilizing the tryptase tetramer interfaces, which leads to dissociation to inactive monomers.

Serine proteases are well-known for their structural plasticity, which is inherent in their mechanism of activation where so-called activation domain loops undergo significant conformational changes from inactive zymogen to active protease (Huber and Bode, 1978). In addition, cofactors are allosteric activators of serine proteases and often needed to achieve optimal active conformations (Gohara and Di Cera, 2011). In tryptase each protomer serves as a cofactor for its neighbor (Maun et al., 2018). Upon anti-tryptase binding to its exosite, allosteric changes occur in structural elements that are important for both small and large tetramer interfaces, as assessed with disulfide-locked dimers (Figure 5H, I). The structure of the complex supports this notion as we see conformational changes at the small (30s loop) and large (60s loop) interfaces (Figure 5F, G). However, we cannot exclude the possibility that STI binding has some effect on these regions as well since active site binders are known to order active sites and neighboring activation domain loops (Gohara and Di Cera, 2011). The precise molecular mechanism underlying the allosteric inhibition by anti-tryptase remains to be elucidated.

In conclusion, we provide genetic and clinical evidence of a potential role for tryptase as a type 2-independent pathogenic mechanism in asthma. *In vitro* and *in vivo* characterization of anti-tryptase described here highlights the potency, specificity, and allosteric mechanism

of inhibition, which accelerates the natural mechanism of tryptase inactivation. Furthermore, anti-tryptase reduces IgE induced systemic anaphylaxis responses in a humanized mouse model. Together with its favorable PK profile and *in vivo* inhibitory activity in nonhuman primates, we provide a scientific rationale for testing anti-tryptase clinically in MC-mediated diseases such as human asthma.

STAR METHODS

LEAD CONTACT AND MATERIALS AVAILABILITY

Further information and request for resources and reagents should be directed to and will be fulfilled by the lead contact, Tangsheng Yi. Investigators may also request materials from Genentech by submitting a request form at www.gene.com/gene/reagents-program/request.do

EXPERIMENTAL MODEL and SUBJECT DETAILS

Mice—NOD.Cg-*Prkdc*^{scid} *Il2rg*^{tm1Wjl}Tg(CMV-IL3,CSF2,KITLG)1Eav/MloySzJ (NOD.*scid IL2rg*^{null} *SCF/GM-CSF/IL3* abbreviated as NSG-SGM3, JAX stock number 013062) were obtained from The Jackson Laboratory. Balb/c mice were obtained from Charles River Laboratories. Female naïve mice, 4–8 weeks old, were used for our studies. Mice were kept in a standard 12 hour light-dark cycle under the specific pathogen free conditions and were allowed free access to sterile food and water. Balb/c mice were healthy and immune-normal. NSG-SGM3 mice were deficient in adaptive immunity to allow human immune cell engraftment but otherwise healthy. All mouse experimentation protocols were approved by the Laboratory Animal Resources Committee at Genentech Inc and adhered to the NIH Guidelines for the Care and Use of Laboratory Animals.

Rabbits—New Zealand white rabbits were obtained from Western Oregon Rabbit Co. and immunization of naïve white rabbits were performed at Epitomics (now an Abcam company) as a fee-for-service. All rabbit experimentation procedures were performed in accordance with animal care and use protocols approved by an Institutional Animal Care and Use Committee (IACUC) at Epitomics.

Cynomolgus monkeys—Cynomolgus monkeys were obtained from Charles River Laboratories. Healthy male cynomolgus monkeys, 3 to 8 years of age, were used for this study and the study protocol was approved by Institutional Animal Care and Use Committee at Charles River Laboratories.

Cell line and primary human cells—LAD2 cells were kindly provided by Dr. Arnold Kirshenbaum from National Institute of Health. LAD2 cells were cultured in a humidified incubator at 37°C with 5% CO_2 in StemPro-34 serum free growth medium containing Stem Pro-34 nutrient supplement (Thermo Fisher Scientific), 1X Penicillin-Streptomycin-Glutamine (Thermo Fisher Scientific) and 100 ng/mL recombinant human SCF (BioLegend). Authentication of LAD2 was validated by human SCF dependent growth and functional release of mast cell mediators (e.g. histamine, PDG2) upon IgE crosslinking.

Normal human bronchial smooth muscle cells and lung fibroblast were obtained from Lonza. Normal Human Lung Fibroblast Cells (Lonza) were cultured in a humidified incubator at 37°C with 5% CO_2 in complete fibroblast growth media, FGM, (Lonza). Assay media is basal FGM culture media (Lonza) without human serum or supplements added. Human Bronchial Smooth Muscle Cells (Lonza) were cultured in a humidified incubator at 37°C with 5% CO_2 in complete culture media SmGM-2 (Lonza). Assay media is SmGm-2 culture media without supplements added (Lonza). Primary human cells were directly ordered from Lonza without additional freeze/thaw and used for experiments under 10 passages.

Enriched $CD34^+$ human cord blood stem cells were obtained from AllCells with more than 80% purity validated by flow cytometry analysis. CHO DKO cell line (Macaraeg et al., 2013) was a derivative of the CHO-K1 cell line (ATCC number CCL-61) was grown and transfected in a Ham's F12/DMEM media (Macaraeg et al., 2013). HEK293 DKO cell line (Arena et al., 2019) was a derivative of HEK293 (ATCC number CRL-1573) and was cultured in Opti-MEM I reduced-serum medium (ThermoFisher) (Arena et al., 2019).

Human subjects and clinical cohorts—Donor foreskins, which otherwise would be disposed of, were provided by pediatricians. Specimens from 245 male subjects (maximum age of 18 years) were included and informed consent of the patients or their legal guardians was obtained. The specimens were provided to the study investigators in a completely anonymous manner. The study was approved by the Ethics Committee of the Charité Universitätsmedizin Berlin and the experiments were conducted according to the Declaration of Helsinki Principles (Babina et al., 2016).

MILLY (ClinicalTrials.gov identifier: NCT00930163) was a randomized, double-blind, placebo-controlled study of lebrikizumab (anti-IL-13) in adults who had asthma that was inadequately controlled despite inhaled glucocorticoid therapy (Corren et al., 2011).

BOBCAT (Jia et al., 2012) was a multicenter observational study conducted in the United States, Canada, and the United Kingdom of 67 adult patients with moderate-to-severe asthma. Inclusion criteria required a diagnosis of moderate-to-severe asthma (confirmed by an FEV_1 between 40% and 80% of predicted value, as well as evidence within the past 5 years of >12% reversibility of airway obstruction with a short-acting bronchodilator or methacholine sensitivity [PC20] <8 mg/mL) that was uncontrolled (as defined by at least 2 exacerbations in the prior year or a score of >1.50 on the ACQ5 while receiving a stable dose regimen [>6 weeks] of a high-dose ICS [>1000 mg fluticasone or equivalent per day]) with or without a LABA.

EXTRA (ClinicalTrials.gov identifier: NCT00314574) was a randomized, double-blind, placebo-controlled study of Xolair (anti-IgE) in subjects 12–75 years old with moderate to severe persistent asthma. Full details of the study design have been published previously (Hanania et al., 2013). In brief, after a 2- to 4-week run-in period, eligible patients were randomized in a 1:1 ratio to receive Xolair or placebo (in addition to high-dose ICS and LABA, with or without additional controller medications) for 48 weeks. Our pharmacogenetic analysis population was a subset of the overall study population (N=309 of

850), as we limited assessments to patients of European ancestry who consented for genetic analyses.

Moderate asthmatic patients and healthy controls were participants in the Study of the Mechanisms of Asthma (MAST; clinicaltrials.gov: NCT00595153) (Simpson et al., 2014). Additional healthy human control blood and DNA samples were obtained through Genentech Healthy Services from Genentech employee donors.

All clinical study participants included in these analyses reviewed and consented to Informed Consent Forms which were reviewed and approved by local Institutional Review Board or Ethics Committees for use of clinical data and biomarker analyses.

METHOD DETAILS

Expression and purification of tryptase—Human α- or β-tryptase genes were individually gene synthesized (Genewiz) and subsequently subcloned into a mammalian expression vector behind a CMV promoter and the HSV secretion signal sequence with an N-terminal His_6-tag, an enterokinase cleavage site directly fused to the mature N-terminus of tryptase, and a C-terminal Flag-tag. Transient transfections of DNA plasmids encoding for the tryptases were performed using CHO DKO cell line (Macaraeg et al., 2013), a derivative of the CHO-K1 cell line (ATCC number CCL-61). DNA transfection was performed with a polyethylenimine (PEI) and DNA mix in Ham's F12/DMEM media. The 10 L culture was incubated at 33°C for 4 days and temperature shifted to 31°C for the remaining 10 days of transfections. A proprietary batch feed supplement containing hydrolysates, amino acids, salts and glucose was added 24 h post-transfection to 20% of final volume.

Monomeric tryptase zymogens were purified for the assembly of active tryptase tetramers. CHO DKO supernatants (10 L) expressing the tryptase zymogens were mixed with 25 mL of Ni-NTA Superflow (Qiagen) resin for batch binding overnight at 4°C. Supernatants and resin mixtures were packed into an XK16 column (GE Healthcare). The column was washed with 3 column volumes (CV) of PBS, pH 7.2 containing 150 mM NaCl, followed by another wash of 5 CV PBS buffer with 300 mM NaCl and 0.01% Triton X114 at the flow rate equivalent to 25% CV/min. The column then underwent a third wash with 10 CV PBS, pH 7.2, plus 150 mM NaCl. The fourth wash used 5 CV of PBS with 300 mM NaCl, pH 7.2 containing 8 mM imidazole to remove non-specific bound proteins. The zymogen was eluted with 250 mM imidazole in PBS, pH 8.0. The elution pool was dialyzed into a buffer of 10 mM MOPS, 250 mM NaCl, at pH 6.0 or pH 6.8.

The assembly of active tryptase tetramers required the cleavage of the N-terminal sequence of the zymogen monomers. Zymogens were concentrated to 5 mg/mL, and the final concentrations of 0.5 mg/mL enterokinase (NEB) and 0.5 mg/mL freshly prepared heparin sodium salt (Sigma-Aldrich) were added to the tryptase zymogen solutions. Mixtures were incubated at room temperature overnight 18–24 h with gentle rotation. The enterokinase-cleaved tryptases (mixtures of tetramers and mature monomers) were then loaded directly onto a 24 mL Superdex 200 10/300 GL column (GE Healthcare) and run in 10 mM MOPS, 2.0 M NaCl, pH 6.0 at 1 mL/min to separate tryptase tetramers from cleaved monomers.

Eluted fractions containing tryptase tetramers were assessed for the tetramer molar mass by size exclusion chromatography (SEC) coupled with multi-angle light scattering (MALS). Tryptase tetramers were pooled after the size was confirmed by SEC-MALS and were then concentrated to 1–3 mg/mL in 10 mM MOPS, 2.0 M NaCl, pH 6.0. Purified tetramers were characterized by SEC-MALS to confirm the purity and tetramer molar mass.

Generation of anti-tryptase antibodies—Both Balb/c mice and New Zealand white rabbits were immunized with either recombinant human monomeric or tetrameric βI-tryptase. Hybridomas were then generated from both the mice and rabbits using standard methods. The resulting supernatants were then screened by ELISA against monomeric βI-tryptase. Briefly, 96-well Maxisorp plates were coated overnight with NeutrAvidin (Thermo Fisher Scientific) at 5 μg/mL and then blocked with PBS with 0.5% bovine serum albumin (BSA) and 0.05% Tween 20 for 30 min. Biotinylated human βI-tryptase (diluted in PBS with 0.5% BSA, 0.05% Tween 20, and 0.1 mg/mL heparin) was added to the wells at 1 μg/mL for 1 h. After three washes, hybridoma supernatants (samples) or controls were added to the wells for 1 h followed by a horseradish peroxidase (HRP) conjugate (1:10,000; goat anti-rabbit IgG (H+L) HRP or goat anti-mouse IgG (H+L) HRP; Thermo Fisher Scientific) for 30 min. The BioFX TMB substrate was added, incubated for 5 min, and quenched with BioFX stop solution. The plates were read at $OD_{650\ nm}$. All ELISA-positive clones were purified by affinity chromatography using standard methods (described more in details in the section of “Expression and purification of anti-tryptase IgG”) and then screened for inhibition of human tryptase activity (described in the section of “tryptase enzymatic activity assays”). The antibody light chain and heavy chain variable domain sequences for the clones with the best inhibitory activity were obtained by RT-PCR.

The humanized 31A clone was generated by inserting the CDR regions of the light and heavy chain domains into the closest human consensus germline and grafting various Vernier positions onto the human germlines. The resulting DNA sequences were codon optimized for human expression, synthesized by Genewiz, and subcloned into mammalian expression vectors. The variable light chain was cloned into a pRK mammalian cell expression vector containing the human kappa constant domain (pRK.LPG3.HumanKappa; Genentech) using sites for AgeI and KpnI. The variable heavy chain was inserted into a pRK mammalian cell expression vector encoding the full-length human IgG4 constant domain (pRK.hIgG4; Genentech) using sites for BsiWI and ApaI. All of the IgG4 antibodies contained the S228P mutation in the heavy chain constant region to prevent Fab-arm exchange.

Expression and purification of anti-tryptase IgG—All the humanized anti-tryptase variants were expressed as IgG4 antibodies in mammalian cells (CHO, CHO DKO (Macaraeg et al., 2013), HEK293 or HEK293 DKO (Arena et al., 2019)). Cells were seeded at 1.0×10^6 cells/mL for transfection and incubated at 37 °C, 5% CO_2 for 2 h prior to transfection. 30 μg of DNA (15 μg of LC and 15 μg of HC) was diluted in a DMEM-based medium to a final volume of 3 mL. Then 60 μL of 7.5 mM 25 kDa linear PEI (Sigma) was added to the DNA solution, mixed and incubated at room temperature before being added to the cells.

Seven days after transfection, the supernatant was harvested and purified using HiTrap column (GE healthcare) with MabSelect Sure resin (GE Healthcare). Phosphate buffered saline (PBS; 0.01 M phosphate, 0.137 M NaCl, pH 7.2) was used as the loading buffer. Antibodies were eluted with 0.1 M citrate, pH 3.0, and neutralized with 3 M Tris, pH 8.0, to a final pH of ~7.0. The eluted antibodies were dialyzed against PBS, pH 7.2, prior to the next purification step. Each antibody was further polished via size exclusion chromatography to remove any aggregates and increase the homogeneity of monomeric antibody to at least 95%. Samples were run on a Superdex S200 10/300 GL size exclusion column column (GE Healthcare) using PBS, pH 7.2, load buffer at a flow rate of 1 mL/min (30 cm/h). Pooled fractions were filtered using a 0.2 μm filter, and antibody monomer content of the final antibody preparation was assessed by analytical SEC carried out with a TSK-GEL, Super SW3000, 4.6 mm × 30 cm, 4 μm (Tosoh Bioscience) column using a Dionex Ultimate 3000 system (Thermo Fisher Scientific) at a flow rate of 0.3 mL/min.

Total tryptase ELISA—Human BAL fluid or plasma tryptase levels were measured using a sandwich ELISA with 2 different monoclonal anti-tryptase antibodies capable of detecting human βI-, βII-, βIII-, and α-tryptases (monomer or tetramer). Recombinant human tetrameric βI-tryptase was used to establish a standard curve. Briefly, 384-well Maxisorp plates (Thermo Fisher Scientific) were coated with capture antibody in PBS overnight at 4°C, washed with PBS plus 0.05% polysorbate-20 (PBST), then blocked with PBS/0.5% BSA for 2 h. This and all subsequent incubations were performed at room temperature with gentle agitation. BAL or plasma samples diluted to a minimum of 1:4 or 1:100, respectively, in assay buffer (1X PBS pH 7.4, 0.35 M NaCl, 0.5% BSA, 0.05% polysorbate-20, 0.25% CHAPS, 5 mM EDTA, 15 PPM Proclin) were added to the plates after washing, and incubated for 2 h. After washing, plates were incubated with biotinylated detection antibody (E82.AS, a chimeric rabbit/human antibody derived from rabbit E82 with the VL-CL disulfide changed to A and S (C80A:C171S), respectively) diluted in assay diluent (1X PBS pH 7.4, 0.5% BSA, 0.05% polysorbate-20, 15 PPM Proclin) for 1 h followed by SA-HRP (1/20,000, GE Healthcare), also for 1 h. After washing, color was developed with tetramethyl benzidine (TMB, Moss) and the reaction was stopped by adding phosphoric acid. The plates were read at 450 nm with a 620 nm reference using a microplate reader. The concentrations of human tryptase were determined from a four-parameter fit of the standard curve. The lower limit of quantification was 5 pg/mL in BAL or 140 pg/mL in plasma. A median albumin value in all asthma samples was used to normalize various dilution factors in BAL. ELISA analysis of BAL albumin was performed as per manufacturer's instructions (Bethyl Laboratories, Inc.). The kit provided human reference serum was used to establish the standard curve. In brief, 384-well plates were coated overnight at 4°C with goat-anti-human albumin antibody (10 μg/mL) in 0.05 M sodium bicarbonate buffer, pH 9.6. Subsequent steps were performed as in the total tryptase ELISA with the exception that standards, BAL samples (minimum 1:100 dilution), and HRP-conjugated goat-anti-human albumin detection antibody (1:30,000 dilution) were all diluted in assay diluent. The lower limit of albumin quantification was 313 ng/mL in BAL.

Active tryptase allele count—PCR followed by Sanger sequencing of genomic DNA was employed to determine active tryptase allele count as described previously (Trivedi et

al., 2009). In brief, active tryptase allele count was assessed as the number of remaining active tryptase genes (encoding βI-, βII-, βIII-tryptases) after accounting for tryptase alleles encoding α- and βIII^{FS}-tryptases (Trivedi and Caughey, 2010). Genotypes were automatically called using the intensity ratio of the two (A/B) alleles. Patients were assigned to genotype bin based on this ratio. Genotypes were confirmed by visual inspection of the sequencing traces for 5% of the population without error. Identification of α-tryptase duplication was performed with whole genome sequencing of blood DNA from asthma patients and the detection algorithm was based on a previous report (Lyons et al., 2016).

Tryptase Genotyping—We used a consensus realignment strategy to assign α and βIII frameshift allele counts to individuals for whom we had Illumina whole genome sequencing (WGS) data. WGS data were aligned against the human reference genome (GRCh38) using bwa according to GATK best practices. We extracted reads aligning to the genomic region including the tryptase genes (chr16:1200000–1300000). Paired end reads from this region were realigned to a consensus sequence derived from the majority of the genic sequence (exons + introns) from the TPSB2, TPSAB1 and TPSD1 genes (see Data S1). Crucially, this region includes the inactivating catalytic triad variant identified in α-tryptase (highlighted in red, Data S1), and the insertion position for the βIII-tryptase frameshift allele (denoted in green, Data S1).

From the alignments to the tryptase consensus, we found evidence of an insertion that corresponded to the frameshift allele in many individuals in our WGS cohort. In order to determine βIII-tryptase frameshift allele count, we counted the number of reads consistent with the frameshift allele, and the total number of reads that aligned against that region of the consensus sequence. The fractional abundance of βIII-tryptase frameshift bearing reads resulted in a trimodal distribution of allele fractions that seemed to indicate presence of 0, 1 or 2 frameshift alleles. When compared against genotyping determined using the Sanger sequencing assay, the estimates determined by the WGS method and the Sanger sequencing results are in accord (Figure S3A, B, C).

α-Tryptase has many single nucleotide variants that differ from tryptase beta alleles, including several SNVs associated with a lack of enzymatic activity. When we performed principal components analysis on the allele fractions for all SNVs in the realigned data, we found that the second principal component correlated with abundance of the known inactivating variants. We identified 43 SNVs that strongly correlated with the second principal component. As with the βIII-tryptase frameshift allele, the average allele fraction showed a roughly trimodal distribution that was indicative of presence of 0, 1 or 2 α-tryptase alleles. These allele count estimates were in strong agreement with α-tryptase allele counts determined by Sanger sequencing (Figure S3A–C).

Examination of the α-tryptase allele fractions identifies a significant number of samples with intermediate fractions that are potentially the result of copy number variation (CNV) of the TPSAB1 gene, as previously described (Lyons et al., 2016). Examination of genomic alignments to the tryptase region in individuals with these unusual allele fractions identified a novel region that potentially indicates the *de novo* junction found in the duplication. We further aligned our tryptase WGS reads against this junction region. Individuals with

evidence of this junction were enriched for intermediate α-tryptase allele fractions. We found a strong association between presence of the junction sequence combined with intermediate allele fraction and SNPs that were previously identified as tagging the TPSAB1 CNV (rs3751664, rs58124832, and rs72552056). We took these SNPs as evidence for tryptase α duplication or triplication and later validated by droplet digital PCR method according to previous description (Lyons et al., 2016). The droplet digital PCR was performed at Gene-by-Gene Inc (Houston, TX) under a service contract between Genentech and Gene-by-Gene.

Affinities and kinetic rates measurement—The affinity of the humanized variants of 31A for each human tryptase was determined by surface plasmon resonance using a Biacore T200 using HBS-P Buffer (GE Healthcare). Biacore Series S CM5 sensor chips were immobilized with monoclonal mouse anti-human IgG (Fc) antibody (Human antibody capture kit from GE Healthcare) and anti-tryptase variants were subsequently captured on each flow cell. Serial 3-fold dilutions of the human tryptase monomer were injected at a flow rate of 30 μL/min. Each sample was analyzed with 3-min association and 10-min dissociation. After each injection the chip was regenerated using 3 M $MgCl_2$. Binding response was corrected by subtracting the RU from a reference flow cell. A 1:1 Languir model of simultaneous fitting of association (k_{on}) and dissociation (k_{off}) rate constants was used for kinetics analysis.

Tryptase enzymatic activity assays—Inhibition of tryptase activity by humanized anti-tryptase antibodies was measured as follows. Recombinant human βI-tryptase tetramer was diluted to 0.75 nM in 200 mM Tris pH 8.0, 150 mM NaCl, 0.1 mg/mL heparin (Sigma-Aldrich), 0.01% TRITON™ X-100), and combined 1:1 with a concentration dependent titration of anti-tryptase antibodies (previously diluted in PBS, pH 7.4) in black ViewPlate 384-F plates (PerkinElmer). Plates were incubated for 1 h at room temperature with gentle agitation. Chromogenic substrate Chromogenix S-2288™ (S-2288) (H-D-lle-Pro-Arg-pNA) (DiaPharma) was diluted to 1.2 mM in the buffer above and added to the plate. Final well concentrations were 400 μM S-2288, 0.25 nM βI-tryptase tetramer, 66 μg/mL heparin (Sigma-Aldrich, and titrated anti-tryptase antibodies. Plates were either read kinetically every 2 min for 60 min or incubated for 40 min at room temperature with gentle agitation and then were read at $OD_{405\ nm}$. Enzymatic activity was linear during the entire assay. IC_{50} values of the anti-tryptase antibodies were determined from a four-parameter fit of their respective curves using Prism (Graphpad).

Tryptase assays at different pH values were carried out as follows. The activity of 1 nM tetrameric βI-tryptase was measured at different pH buffers (50 mM MES pH 6.0, 50 mM Tris for pH 7.0 and 8.0) containing 150 mM NaCl and 1 μg/mL heparin (Sigma-Aldrich) with 1 mM S-2288 substrate (DiaPharma); final volume was 200 μL. Prior to substrate addition, tryptase was incubated for 30 min with either 500 nM anti-tryptase alone or in combination with 2 μM aprotinin (Sigma-Aldrich) or no inhibitors. The reaction velocity was determined by the rate at which p-nitroaniline (pNA) is released, which was measured spectrophotometrically at 405 nm using a SpectraMax M5e plate reader

(Molecular Devices). Experiments were performed in triplicates and velocities reported as means ± SD.

Tryptase assays using different *p*-nitroanilide chromogenic substrates (Table S4) were carried out using 1 nM βI-tryptase tetramer in the absence or presence of 500 nM 31A.v11 IgG4 for 30 min in 50 mM Tris pH 7.5, 150 mM NaCl and 10 μg/mL heparin (Sigma-Aldrich). Assays were initiated by addition of substrate to give a final concentration of 1 mM. Reaction velocities were determined as described above.

Kinetics to determine the of mode of inhibition were carried out using 1 nM βI-tryptase tetramer in 50 mM Tris pH 7.5, 150 mM NaCl, 100 μg/mL heparin (Sigma-Aldrich). Prior to substrate addition, tryptase and anti-tryptase were incubated for 30 min. Reactions were initiated using S-2288 substrate (DiaPharma) with concentrations ranging from 1000 to 0.5 μM at 7 different antibody concentrations ranging from 20 nM to 0.31 nM; final volume was 200 μL. Reaction velocities were determined described as above. Using Kaldeidagraph 4.1.3 (Synergy Software), the velocities were fit to Michaelis-Menten equation using linear regression and K_M and V_{max} values were calculated for each antibody concentration. Experiments were performed in triplicates and data at specific concentrations are mean with standard deviation (SD).

Tryptase assays were carried out using a highly fluorescence quenched protein substrate BODIPY FL-casein (EnzChek Protease Assay Kit, Thermo Fisher Scientific). βI-tryptase tetramer (10 nM) and anti-tryptase (500 nM) were incubated for 30 min in 50 mM Tris pH 7.5, 150 mM NaCl and 10 μg/mL heparin followed by the addition of BODIPY FL-casein (10 μg/mL final concentration). The activity of tryptase was measured by monitoring the fluorescence on a SpectraMax M5e plate reader (Molecular Devices) with excitation at 485 nm and emission at 530 nm.

The endogenous human tryptase from degranulated mast cell supernatant was quantified using a human total tryptase ELISA. The endogenous tryptase was diluted to 2.4 nM in 200 mM Tris pH 8.0, 150 mM NaCl, 0.1 mg/mL heparin (Sigma-Aldrich), 0.01% TRITON™ X-100 and combined at a 1:1 ratio with anti-tryptase antibody or Fab in black Optiplate-384 plates. The plates were incubated for 1 h at room temperature with gentle agitation. A fluorescence-quenched peptide substrate, Mca-Arg-Pro-Lys-Pro-Val-Glu-Nval-Trp-Arg-Lys(Dnp)-NH_2 (ES002, R&D Systems), was diluted to 10.5 μM in enzymatic assay buffer and added to the plates. Final in-well concentrations of the anti-tryptase antibodies, endogenous human tryptase, and ES002 substrate were 0.05–222 nM, 0.8 nM, and 3.5 μM, respectively. The plates were read kinetically every 2 min for 60 min using excitation wavelength at 320 nm to measure the emission at 405 nm. The 100% tryptase activity was determined by the average velocity of the control wells without the antibody and the 0% activity was determined by the average velocity of the control wells without mast cell supernatant.

BAL fluid from murine model of mast cell induced anaphylaxis response was incubated with of 10 μg/ml STI and 5 μM α−1 antitrypsin for 10 min at room temperature in 50 mM Tris

pH 8.0 150 mM NaCl and 1 μg/ml heparin, prior to the addition of 400 μM S-2288. Samples were incubated overnight and read at $OD_{405\ nm}$.

Tryptase enzymatic activity from human mast cells—Primary mast cells were purified from human newborn foreskin ($N = 101$) using anti-human c-Kit microbeads (Miltenyi Biotec) (Babina et al., 2016). Non-mast cell fractions were used for genomic DNA isolation and tryptase genotyping. Tryptase activity was assessed from mast cell lysates using Z-Gly-Pro-Arg-pNA (Bachem) in the presence of α1-antitrypsin (Sigma-Aldrich) to suppress other trypsin-like proteases. Tryptase activity is expressed as a function of equivalent concentration of active tryptase per mast cell.

BSMC collagen contraction assay—Tryptase induced muscle contraction was studied by plating bronchial smooth muscle cells (BSMC; Lonza) in collagen at 9×10^6 cells/mL in a 24-well plate following the manufacturer's guidelines (Cell BioLabs Inc.). After 1 h incubation at 37°C, cells in collagen matrices were overlaid with 1 mL of SmGM-2 without serum or supplements. After 24 h, media was replaced with serum free media. Tetrameric βI-tryptase was diluted in the presence or absence of anti-tryptase (300 μg/mL) and incubated for 30 min at 37°C prior to adding to the specified wells. Final concentrations were 330 nM (10 μg/mL) tryptase and 2 μM (300 μg/mL) anti-tryptase. Cell contraction was initiated by the release of the matrix from the plate wall using a sterile pipette tip. Serum free media alone was used as a no stimulation control. At the start of cell contraction, matrices were visualized, imaged and recorded using a Protein Simple Alpha I Imager. Cells were incubated at 37°C for an additional 3 h and matrices were reimaged and recorded.

Quantification of mast cell degranulation *in vitro*—Anti-NP IgE (100 ng/mL) (JW8.5.13, Serotec) was added to LAD2 cells plated at 4×10^6 cells / 4mL in a 6-well tissue culture plate (Corning) and the cells were incubated overnight at 37°C to prime the cells. Cells cultured in media only, without the addition of anti-NP IgE, served as a negative control. After the overnight incubation, cells were washed three times with media to remove unbound anti-NP IgE. Cells were incubated with 100 μg/mL anti-tryptase or 10 mM tryptase small molecule inhibitor (BMS-262084) (Sutton et al., 2002), mixed thoroughly and incubated at RT for 1 h. Following this incubation, NP-BSA (Sigma) was added to the indicated samples at a final concentration of 0.1 μg/mL to trigger cell degranulation. Samples were mixed thoroughly and incubated at 37°C in CO_2 incubator for 1 h. After 1 h incubation, cells were centrifuged at 3000 rpm for 5 min at RT, and the supernatant was collected for histamine measurement. The cell pellet was lysed using 0.5% Triton X-100. Histamine in the degranulation supernatant was quantitated using histamine ELISA kits (GenWay Biotech, Inc; Neogen Life Sciences).

For human tryptase mediated mast cell degranulation, LAD2 cells were treated with 3 μg/mL tetrameric tryptase (wild-type or S195A mutant) or 3 μg/mL tryptase which had been pre-incubated with 100 μg/mL anti-tryptase for 45 min at room temperature. PBS was added to the specified sample to serve as a no stimulation control. Samples were mixed thoroughly and incubated at 37°C for 1 h. After 1 h incubation, cells were centrifuged at 3000 rpm for 5 min at room temperature, and the supernatant was collected for histamine measurement. Histamine in the degranulation supernatant was quantitated as above.

Prostaglandin D2 was measured in the cell supernatant using a PGD2 ELISA (Cayman). β-hexosamindase release was measured by using the hexosaminidase substrate, p-Nitrophenyl-N-acetyl-β-D-glucosaminde (PNAG dissolved in 0.1M citric acid, pH 4.5). Cell supernatant was combined with prewarmed PNAG substrate in a 96 well plate and incubated at 37C for 2–3 hrs. Total β-hexosaminidase was also measured in the cell pellet. The reaction was stopped with 0.2M glycine-NaOH pH10.8) and OD read at 405 nM with 655 nM as reference. β-hexosaminidase data is expressed as the percent of the total released plus cell pellet.

BSMC proliferation assay—To analyze the proliferative effects of tryptase, BSMC were plated in 96-well tissue culture plates (Corning) at 2×10^5 cells/mL and incubated for 24 h. Cells were treated with serum free media for 24 h. Tetrameric βI-tryptase diluted in the presence or absence of anti-tryptase was added to the cells. Cells treated with media alone were used as a no stimulation control. Final concentrations were 100 nM (3 μg/mL) tryptase and 3 μg/mL to 300 μg/mL anti-tryptase. Plates were incubated for 24 h at 37°C before the addition of 1 μCi of H^3-thymidine per well. Proliferation was measured after 6 h by H^3-thymidine incorporation. Cell-associated radioactivity was quantified by scintillation counting.

Procollagen Type I C-Peptide cell-based assay—Normal primary human lung fibroblasts (NHLF; Lonza) were plated in a 24-well plate at 4×10^4 cells/mL in complete fibroblast growth media (Lonza). After a 24 h incubation, cells were treated with 100 nM (3 μg/mL) tetrameric βI-tryptase alone or βI-tryptase preincubated with 667 nM (100 μg/mL) anti-tryptase for 30 min, 37°C. After 4 days at 37°C, supernatants were quantitated for tryptase induced collagen production using Procollagen Type I C-Peptide EIA (Takara Bio).

Tryptase cleavage of protein substrates—$CD34^+$ culture derived mast cells were primed for 24 h with 2 μg/mL human anti-NP IgE (clone JW8.5.13) and washed with 3 times with growth media. Cells were resuspended in 100 μL of 50 mM Tris pH 8.0, 150 mM NaCl, 0.1 mg/mL heparin (Sigma-Aldrich) at 5×10^5 cells/mL. Degranulation was triggered by incubating cells with 1 μg/mL anti human IgE (Millipore) for 1 h at 37°C. Mast cell degranulation supernatant was incubated in the presence or absence of 200 nM (30 μg/mL) anti-tryptase for 1 h at 37°C prior to the addition of 2 μg vasoactive intestinal peptide (VIP). Samples were incubated for 1 h at 37°C. Samples were then boiled for 5 min and resolved on a Novex 18% Tris Glycine gel (Thermo Fisher Scientific) and stained with SimplyBlue SafeStain (Thermo Fisher Scientific) for protein visualization. Mast cell supernatant without anti-tryptase added, served a stimulation control. Human IgE primed, but not anti IgE triggered, mast cells served as a no stimulation control.

For fibrinogen degradation, 30 nM (1.0 μg/mL) βI-tryptase was preincubated with 1.3 μM (200 μg/mL) anti-tryptase for 30 min in 50 mM Tris, 150 mM NaCl, 0.1 mg/mL heparin (Sigma-Aldrich) at pH 6.0 or 7.5 at room temperature. The mixture was then incubated with 5 μg human fibrinogen (Haematologic Technologies, Inc.) for 2.5 h at 37°C. The resulting cleavage products were resolved on a Novex 8% Tris Glycine gel (Thermo Fisher Scientific), visualized by SimplyBlue SafeStain (Thermo Fisher Scientific) and imaged with a Protein Simple Alpha I Imager.

Size exclusion chromatography—Size exclusion chromatography (SEC) was used to analyze WT and mutant βI-tryptase variants alone or bound to anti-tryptase Fab (humanized 31A.v11) using an Superdex 200 10/300 GL column (25-mL bed volume; GE Healthcare) in either 10 mM MOPS, pH 6.8, 2 M NaCl or 50 mM Tris, pH 8, 150 mM NaCl, 0.1 mg/mL heparin (Sigma-Aldrich) at 0.5 mL/min flow rate and following the absorbance at 280 nm essentially as described (Maun et al., 2018).

Hydrogen-deuterium exchange mass spectrometry—Deuterium uptake rates of monomeric βI-tryptase in the presence and absence of anti-tryptase Fab were measured to determine structural regions modified upon antibody binding. Bound samples contained 1:1 mixture of βI-tryptase and Fab, prepared and incubated at room temperature for 1 h. βI-Tryptase concentration prior to deuterium labeling was 30 μM in Fab bound and unbound samples. HDX experiments consisted of diluting samples 15-fold into deuterium labeling buffer containing 20 mM histidine (Serva Electrophoresis GmbH) buffered with acetic acid to pD 7.0. Six labeling times, logarithmically sampled between 30 s and 1000 min were taken in triplicate, quenched by lowering the pH to pH 2.5 and the addition of 2 M guanidinium chloride (Sigma-Aldrich) and 0.25 M TCEP (Sigma-Aldrich) and injected into a cold online system as described (Mayne et al., 2011).

Briefly, samples were first passed through an immobilized pepsin column (2.1 × 30 mm, Applied Biosystems) and loaded onto an Acquity Vanguard C_8 trap column (Waters) for desalting. Peptide fragments were then separated by reversed-phased chromatography using an Acquity UPLC BEH C_{18} (1.7 μm particle size, 1.0 × 50 mm) (Waters) and introduced into a Thermo Orbitrap Elite mass spectrometer (120k Hz resolution at m/z 400) (Thermo Fisher Scientific) for mass analysis. Chromatographic mobile phases were prepared as described (Walters et al., 2012) to minimize deuterium back exchange. The ExMS program (Kan et al., 2013) as used to identify deuterated peptides and prepare extracted ion chromatograms, which were then analyzed by in-house python scripts (Walters et al., 2013). These scripts combine degenerate charge states, fit isotopic distributions with binomials, and extract the number of deuterium atoms carried, on average, by each peptide.

Crystallization and structural determination—Tetrameric βI-tryptase used for crystallization was expressed in baculovirus-infected *Trichoplusia ni* insect cells (Expression Systems) and purified in a previously described protocol (Maun et al., 2018). Briefly, insect cell media containing secreted His6-tagged zymogen β-tryptase was loaded onto a 10 ml Ni-NTA Superflow column (Qiagen) at a volumetric flow rate of 170 cm/h. The column was washed with 10 column volumes (CV) of wash buffer (20 mM Tris pH 8, 10 mM imidazole, 300 mM NaCl) and eluted with 8 CV elution buffer (20 mM Tris pH 8, 300 mM imidazole, 300 mM NaCl). Fractions assayed by SDS-PAGE containing β-tryptase were pooled, concentrated and loaded onto an Superdex 200 10/300 GL size exclusion column (GE Healthcare) for further purification by size-exclusion chromatography (SEC) using buffer (10 mM MOPS pH 6.8, 2 M NaCl) at a flow rate of 0.5 mL per minute. Fractions containing zymogen β-tryptase (monomeric) were pooled and concentrated. Zymogen β-tryptase was then cleaved overnight at room temperature at a concentration of 2 mg/ml in 10 mM MOPS pH 6.8, 0.2 M NaCl containing 0.5 mg/ml heparin sodium salt (Sigma-Aldrich)

and 0.1 mg/ml enterokinase (NEB). Tetrameric β-tryptase was then subjected to SEC in buffer (10 mM MOPS pH 6.8, 2 M NaCl) to purify tetrameric β-tryptase by removing EK and any uncleaved zymogen β-tryptase.

For crystallization, Tetramer βI-tryptase was mixed with 1.5-fold molar excess anti-tryptase Fab (humanized 31A.v11) and 2-fold molar excess soybean trypsin inhibitor (STI) (Sigma-Aldrich) and incubated for 10 min at room temperature. The mixture was then subjected to size exclusion chromatography using an S200GL column (GE Healthcare) in 10 mM MOPS pH 6.8, 0.5 M NaCl. Fractions containing the ternary complex of Fab, βI-tryptase and STI were pooled and concentrated to 40 mg/mL.

Crystallization buffer containing 0.1 M Tris pH 7.5, 0.2 M lithium sulfate and 5% PEG4000 was mixed in equal volume with protein solution. Crystals of βI-tryptase•Fab•STI were grown at 19°C using vapor diffusion in hanging drops. The crystals were dipped in artificial mother liquor containing 25% ethylene glycol and vitrified in liquid nitrogen.

Diffraction data extending to 2.15 Å were collected in a hexagonal lattice at ALS beamline 5.0.2. Data reduction and scaling (Otwinowski Z, 1997; Winn et al., 2011) allowed assignment of the Laue class to 6/mmm. Based on unit cell volume and proposed protein content, a single βI-tryptase•Fab•STI complex was expected in the crystallographic asymmetric unit. The structure was solved using molecular replacement (McCoy et al., 2007) in space group $P6_222$ using as search probes a previously determined tryptase protomer derived from PDB accession 4A6L (Liang et al., 2012) STI from PDB 1AVU (Song and Suh, 1998), an Fv fragment stripped of CDR loops from PDB 1FVC (Eigenbrot et al., 1993), and the constant region from PDB 1FVD, each as separate bodies. After some restrained refinement (Murshudov et al., 2011), electron density maps permitted correction of Fab protein sequence and fitting missing residues and side chains into clear density (Emsley et al., 2010). Waters were added automatically (Adams et al., 2010). More rounds of model adjustments and refinement (Bricogne G, 2011) led to the final model, metrics for which appear in Table S4. The model is continuous for βI-tryptase residues I16-K244 (chymotrypsinogen numbering), STI residues D1-D177, Fab light chain residues D1-C214 (Kabat numbering). The Fab heavy chain is continuous except for a five amino acid residue gap in the constant domain. The value for the shape complementarity statistic (Sc) (Lawrence and Colman, 1993) is 0.73, consistent with other tight-binding Fab/antigen complexes. Solvent accessible surface area calculations were carried out using XSAE (personal communication from C. Broger, F. Hoffman-LaRoche, Basel). Crystal packing contacts ≤ 4 Å are well distributed around STI, tryptase, and all four Fab domains and include numerous H-bonds as well as hydrophobic contacts.

Murine model of mast cell induced anaphylaxis—NSG-SGM3 mice were irradiated with 100 cGy and reconstituted with $CD34^+$ human hemopoietic stem cells (performed at Jackson Laboratory). Twelve weeks after reconstitution, human immune cell engraftment was confirmed by flow cytometry analysis of blood human $CD45^+$ cells and frequency of $CD117^+FcεRI^+$ mast cells and serum human tryptase ELISA. Induction of IgE mediated anaphylaxis was performed as described (Bryce et al., 2016). Animals (groups of 8–10) with similar blood mast cell percentage from the same human donor were re-randomized

into two groups based on the similar engraftment rate of human mast cells in blood and injected intravenously (IV) with anti-tryptase (250 μg/mice) or anti-gD IgG4 (250 μg/mice) respectively. After antibody treatment for 6 h, all animals were injected IV with 5 μg of anti-NP IgE (JW8.5.13, Serotec). Systemic anaphylaxis was induced 12 h later by an IV injection of NP-BSA conjugates (Sigma) and body temperature was monitored for every 5–10 min.

Pharmacokinetics in cynomolgus monkeys—To evaluate the pharmacokinetics and pharmacodynamics of anti-tryptase in nonhuman primates, six male cynomolgus monkeys (*Macaca fascicularis*, Chinese origin) were assigned to 2 groups (n = 3/group). The animals were approximately 3–4 years old and weighed approximately 3.4–4.4 kg at the initiation of the study. Animals in group 1, were given a single 30 mg/kg IV bolus dose of anti-gD antibody (isotype control), and animals in group 2 received a 30 mg/kg single IV dose of anti-tryptase. Doses were administered via the saphenous vein. At various timepoints up to 43 days post-dose, serum samples (n = 3 samples/timepoint) were collected and analyzed for serum anti-tryptase concentrations by ELISA methods. Individual serum concentration at different time point were used to estimate pharmacokinetic parameters using a two-compartmental and non-compartmental analysis. Levels of active tryptase and total tryptase were evaluated in the BAL fluid collected on study Days −6, 1 (8 h post-dose), 3, 8, 15, 22, and 29, and measured as a PD biomarker to assess target engagement in animals.

Active tryptase quantification—Cynomolgus monkey active tryptase levels from BAL fluid and human active tryptase levels in BAL fluid from humanized mice were measured using a sandwich ELISA (Figure S5). An antibody recognizing cynomolgus monkey tryptase (13G6) or human tryptase (E88.AS, a chimeric rabbit/human antibody derived from rabbit E88 with the VL-CL rabbit disulfide changed to A and S (C80A:C171S), respectively) was used as the capture antibody and active recombinant cynomolgus monkey or human tryptase tetramers were used to establish a standard curve. Assay standards, controls, and diluted samples were incubated for 10 min with 0.5 mg/mL STI (Sigma-Aldrich) and then labeled with 1 μM of a biotinylated activity-based probe (ABP) - Bio-PK-DPP (probe 4), which binds covalently to the active form of tryptase, for 1 h (Pan et al., 2006). A small molecule tryptase inhibitor (BMS-262084) (Sutton et al., 2002) was then added at 10 μM for 20 min to stop the ABP labeling followed by incubation with 10 μg/mL of anti-tryptase antibody for 10 min. The mixture was added to an ELISA plate pre-coated with the capture antibody, incubated for 1 h, washed with PBST and incubated with streptavidin horseradish peroxidase (SA-HRP; GE Healthcare) for 2 h. After washing, color was developed with TMB (SeraCare) and the reaction was stopped by adding phosphoric acid. Plates were read at 450 nm/630 nm using a Molecular Devices Spectramax M3 microplate reader. The lower limit of quantification (LLOQ, 0.078 ng/mL) in the 1:2 dilution of cynomolgus monkey BAL samples is denoted by a dotted line. Data points falling below LLOQ were plotted as 0.04 ng/mL, which was half the LLOQ of the assay. For detection of active human tryptase in mouse BAL fluid the lower limit of quantification (LLOQ, 0.3 ng/ml) is denoted by a dotted line. Data points falling below LLOQ were plotted as 0.15 ng/ml, which was half of the LLOQ of the assay.

Additional characterization was performed to ensure specificity of binding of ABP to active tryptase (Figure S5). Recombinant cynomolgus monkey active tryptase was pretreated with a tryptase small molecule inhibitor (10 μM BMS-262084) or 10 μg/ml dissociating anti-tryptase antibody (31A.v11) for 30 min prior to labeling with 10 μM biotinylated-ABP for 20 min. Samples (in reducing loading buffer) were run on a 4–12% BT/MES denaturing gel. Gel was visualized by Western blot with streptavidin horseradish peroxidase (at 1:5000; GE Healthcare) for 45 min. The blot was stripped and re-blotted for total tryptase with antibody AA1 (Thermo Fisher Scientific), which recognizes total tryptase (at 1:1000), for 2 h; detection was carried out with West dura reagent (Thermo Fisher Scientific).

Cynomolgus monkey *Ascaris suum*—Cynomolgus monkeys were sensitized by challenges with *Ascaris suum* (*A. suum*) by: intra-muscular injection on days 0, 7, 15, 34, 71, 78, and 85; intra-peritoneal injection on days 0, 7, 15, 71, 78, and 85; and inhalation on days 29, 50, 120, 184, and 205. This sensitization procedure was based on a previous study as described (Iwashita et al., 2008). For *A. suum* inhalation, animals were anesthetized, intubated, and mechanically ventilated. A single dose of *A. suum* (between 4 or 4000 μg/mL in PBS; appropriate concentration for each animal was determined during sensitization phase as the concentration which elicited desired/adequate lung reactivity) was administered via intermittent positive pressure breathing with a ventilator and in-line nebulizer over 30 breaths. Seven monkeys with positive response as determined by wheal/flare response to intra-dermal *A. suum* challenge on day 140 and lung function response to inhaled *A. suum* challenge on day 205 were used in this study.

Each animal underwent a vehicle treatment phase and a drug treatment phase. Therefore, each animal serves as its own control (see Figure 7E). During the vehicle phase, animals were administered vehicle (20 mM histidine acetate/240 mM sucrose, pH 5.5) via slow IV bolus injection (Day 1). Twenty-four hours following vehicle administration (Day 2), each animal received an inhaled challenge with *A. suum*. BAL samples were collected 30 min after challenge and used for measurement of active tryptase. Animals were rested for 4 weeks prior to start of the drug phase of the study. During the drug phase, the same animals were administered anti-tryptase antibody (100 mg/kg) via slow IV bolus injection on Day 1. Twenty-four hours following vehicle administration (Day 2), each animal received an inhaled challenge with *A. suum*. BAL samples were collected 30 min after challenge and used for measurement of active tryptase. In the BAL of one animal there was a non-specific signal that interfered in the active tryptase immunoassay, which confounded the ability to assess active tryptase in this animal.

Quantitation of 3-methyl histamine in cynomolgus monkey urine was achieved using a liquid chromatography coupled with mass spectrometry. Chromatographic separation was achieved by using a Phenomenex Luna HILIC column (50×2.1 mm, 2.7 μm) with gradient elution using 25mM ammonium formate in 50:50 acetontrile:water and 25 mM ammonium formate in 95:5 acetonitrile:water with a flow rate of 0.8 ml/minute. The retention times were 0.99 minutes for both 3-methyl histamine and 3-methyl histamine-d3 (internal standard) and multiple reaction monitoring used 126.0 -> 109 m/z for 3-methylhistamine and 129.1 -> 112.1 m/z for 3-methyl histamine-d3.

Collection of bronchoalveolar lavage fluid—The bronchoalveolar lavage (BAL) fluid was collected by guiding a pediatric fiberoptic bronchoscope past the carina to wedge in a major bronchus. Pre-warmed 20 mL PBS was instilled and immediately aspirated for collection into a 50 mL conical tube. Samples were placed on ice until they were centrifuged at 1500–1700 RPM for 10–12 min at 2–8°C. Supernatants were collected and stored at −60 to −80°C.

QUANTIFICATION AND STATISTICAL ANALYSIS

R software (version 3.4.3) and R packages (haven, lme4, lsmeans, contrast, and multcomp) was utilized for data analysis and plotting for Figure 1, 2, 3. The statistical methods are described in the text and figure and table legends.

GraphPad Prism was utilized for statistical analysis on Figure 4–7. Statistical details of experiments can be found in figure legends or table description, including the statistical tests used and value and definition of n.

Differences were considered to be statistically significant when $p < 0.05$. For clinical samples analysis, all available subjects are included in the analysis. For biological experiments, sample sizes were determined based on previous experience with similar experiments.

DATA AND CODE AVAILABILITY

The accession number for the Atomic coordinates for anti-tryptase Fab•βI-tryptase•STI ternary complex is PDB: 6O1F. Further information about sample preparation, data collection, or data processing is described in the method details and can also be directed to the Lead Contact.

ADDITIONAL RESROUCES

Web resources containing the clinical trial design and enrollment criteria can be in ClinicalTrials.gov. Registry number for MAST study is NCT00595153. Registry number for EXTRA study is NCT00314574. Registry number for MILLY STUDY is NCT00930163.

Supplementary Material

Refer to Web version on PubMed Central for supplementary material.

Acknowledgements

We thank Menno van Lookeren Campagne, Rick Brown, and Elaine Chang for the critical input on the project, Ryan Abraham and Phil Hass for purification of antibody for the cynomolgus monkey study, Julia Gray for help analyzing the antibody concentration in cynomolgus monkeys. LAD2 cells were kindly provided by Drs. Arnold Kirshenbaum and Dean Metcalfe (NIH).

References

Adams PD, Afonine PV, Bunkoczi G, Chen VB, Davis IW, Echols N, Headd JJ, Hung LW, Kapral GJ, Grosse-Kunstleve RW, et al. (2010). PHENIX: a comprehensive Python-based system for

macromolecular structure solution. Acta Crystallogr D Biol Crystallogr 66, 213–221. [PubMed: 20124702]

Alter SC, Kramps JA, Janoff A, and Schwartz LB (1990). Interactions of human mast cell tryptase with biological protease inhibitors. Archives of biochemistry and biophysics 276, 26–31. [PubMed: 1688695]

Alter SC, Metcalfe DD, Bradford TR, and Schwartz LB (1987). Regulation of human mast cell tryptase. Effects of enzyme concentration, ionic strength and the structure and negative charge density of polysaccharides. The Biochemical journal 248, 821–827. [PubMed: 2449172]

Arena TA, Chou B, Harms PD, and Wong AW (2019). An anti-apoptotic HEK293 cell line provides a robust and high titer platform for transient protein expression in bioreactors. MAbs 11, 977–986. [PubMed: 30907238]

Babina M, Guhl S, Artuc M, Trivedi NN, and Zuberbier T (2016). Phenotypic variability in human skin mast cells. Exp Dermatol 25, 434–439. [PubMed: 26706922]

Berger P, Perng DW, Thabrew H, Compton SJ, Cairns JA, McEuen AR, Marthan R, Tunon De Lara JM, and Walls AF (2001). Tryptase and agonists of PAR-2 induce the proliferation of human airway smooth muscle cells. J Appl Physiol (1985) 91, 1372–1379. [PubMed: 11509538]

Berry M, Morgan A, Shaw DE, Parker D, Green R, Brightling C, Bradding P, Wardlaw AJ, and Pavord ID (2007). Pathological features and inhaled corticosteroid response of eosinophilic and non-eosinophilic asthma. Thorax 62, 1043–1049. [PubMed: 17356056]

Bradding P, and Brightling C (2007). Mast cell infiltration of airway smooth muscle in asthma. Respir Med 101, 1045; author reply 1046–1047. [PubMed: 17306523]

Bricogne G, B. E, Brandl M, Flensburg C, Keller P, Paciorek W, Roversi P, Sharff A, Smart OS, Vonrhein C, Womack TO (2011). BUSTER version 2.11.2. (Cambridge, United Kingdom: Global Phasing Ltd.).

Brightling CE, Bradding P, Symon FA, Holgate ST, Wardlaw AJ, and Pavord ID (2002). Mast-cell infiltration of airway smooth muscle in asthma. N Engl J Med 346, 1699–1705. [PubMed: 12037149]

Bryce PJ, Falahati R, Kenney LL, Leung J, Bebbington C, Tomasevic N, Krier RA, Hsu CL, Shultz LD, Greiner DL, et al. (2016). Humanized mouse model of mast cell-mediated passive cutaneous anaphylaxis and passive systemic anaphylaxis. J Allergy Clin Immunol 138, 769–779. [PubMed: 27139822]

Cairns JA, and Walls AF (1997). Mast cell tryptase stimulates the synthesis of type I collagen in human lung fibroblasts. J Clin Invest 99, 1313–1321. [PubMed: 9077541]

Cohn L, Elias JA, and Chupp GL (2004). Asthma: mechanisms of disease persistence and progression. Annu Rev Immunol 22, 789–815. [PubMed: 15032597]

Corren J, Lemanske RF, Hanania NA, Korenblat PE, Parsey MV, Arron JR, Harris JM, Scheerens H, Wu LC, Su Z, et al. (2011). Lebrikizumab treatment in adults with asthma. N Engl J Med 365, 1088–1098. [PubMed: 21812663]

Cui Y, Dahlin JS, Feinstein R, Bankova LG, Xing W, Shin K, Gurish MF, and Hallgren J (2014). Mouse mast cell protease-6 and MHC are involved in the development of experimental asthma. J Immunol 193, 4783–4789. [PubMed: 25320274]

Dougherty RH, Sidhu SS, Raman K, Solon M, Solberg OD, Caughey GH, Woodruff PG, and Fahy JV (2010). Accumulation of intraepithelial mast cells with a unique protease phenotype in T(H)2-high asthma. The Journal of allergy and clinical immunology 125, 1046–1053 e1048. [PubMed: 20451039]

Dvorak AM, McLeod RS, Onderdonk A, Monahan-Earley RA, Cullen JB, Antonioli DA, Morgan E, Blair JE, Estrella P, Cisneros RL, et al. (1992). Ultrastructural evidence for piecemeal and anaphylactic degranulation of human gut mucosal mast cells in vivo. Int Arch Allergy Immunol 99, 74–83. [PubMed: 1483068]

Eigenbrot C, Randal M, Presta L, Carter P, and Kossiakoff AA (1993). X-ray structures of the antigen-binding domains from three variants of humanized anti-p185HER2 antibody 4D5 and comparison with molecular modeling. Journal of molecular biology 229, 969–995. [PubMed: 8095303]

El-Shazly A, Berger P, Girodet PO, Ousova O, Fayon M, Vernejoux JM, Marthan R, and Tunon-de-Lara JM (2006). Fraktalkine produced by airway smooth muscle cells contributes to mast cell recruitment in asthma. J Immunol 176, 1860–1868. [PubMed: 16424217]

Elrod KC, Moore WR, Abraham WM, and Tanaka RD (1997). Lactoferrin, a potent tryptase inhibitor, abolishes late-phase airway responses in allergic sheep. Am J Respir Crit Care Med 156, 375–381. [PubMed: 9279212]

Emsley P, Lohkamp B, Scott WG, and Cowtan K (2010). Features and development of Coot. Acta Crystallogr D Biol Crystallogr 66, 486–501. [PubMed: 20383002]

Fahy JV (2015). Type 2 inflammation in asthma--present in most, absent in many. Nat Rev Immunol 15, 57–65. [PubMed: 25534623]

Franconi GM, Graf PD, Lazarus SC, Nadel JA, and Caughey GH (1989). Mast cell tryptase and chymase reverse airway smooth muscle relaxation induced by vasoactive intestinal peptide in the ferret. J Pharmacol Exp Ther 248, 947–951. [PubMed: 2495355]

Fukuoka Y, and Schwartz LB (2006). The B12 anti-tryptase monoclonal antibody disrupts the tetrameric structure of heparin-stabilized β-tryptase to form monomers that are inactive at neutral pH and active at acidic pH. Journal of immunology (Baltimore, Md : 1950) 176, 3165–3172.

Galli SJ, and Tsai M (2012). IgE and mast cells in allergic disease. Nat Med 18, 693–704. [PubMed: 22561833]

Gaudenzio N, Sibilano R, Marichal T, Starkl P, Reber LL, Cenac N, McNeil BD, Dong X, Hernandez JD, Sagi-Eisenberg R, et al. (2016). Different activation signals induce distinct mast cell degranulation strategies. The Journal of clinical investigation 126, 3981–3998. [PubMed: 27643442]

Gohara DW, and Di Cera E (2011). Allostery in trypsin-like proteases suggests new therapeutic strategies. Trends in biotechnology 29, 577–585. [PubMed: 21726912]

Haldar P, Brightling CE, Hargadon B, Gupta S, Monteiro W, Sousa A, Marshall RP, Bradding P, Green RH, Wardlaw AJ, et al. (2009). Mepolizumab and exacerbations of refractory eosinophilic asthma. N Engl J Med 360, 973–984. [PubMed: 19264686]

Hallgren J, Estrada S, Karlson U, Alving K, and Pejler G (2001). Heparin antagonists are potent inhibitors of mast cell tryptase. Biochemistry 40, 7342–7349. [PubMed: 11401583]

Hallgren J, Lindahl S, and Pejler G (2005). Structural requirements and mechanism for heparin-dependent activation and tetramerization of human betaI- and betaII-tryptase. Journal of molecular biology 345, 129–139. [PubMed: 15567416]

Hallgren J, and Pejler G (2006). Biology of mast cell tryptase. An inflammatory mediator. The FEBS journal 273, 1871–1895. [PubMed: 16640553]

Hanania NA, Alpan O, Hamilos DL, Condemi JJ, Reyes-Rivera I, Zhu J, Rosen KE, Eisner MD, Wong DA, and Busse W (2011). Omalizumab in severe allergic asthma inadequately controlled with standard therapy: a randomized trial. Ann Intern Med 154, 573–582. [PubMed: 21536936]

Hanania NA, Wenzel S, Rosen K, Hsieh HJ, Mosesova S, Choy DF, Lal P, Arron JR, Harris JM, and Busse W (2013). Exploring the effects of omalizumab in allergic asthma: an analysis of biomarkers in the EXTRA study. Am J Respir Crit Care Med 187, 804–811. [PubMed: 23471469]

He S, Aslam A, Gaca MD, He Y, Buckley MG, Hollenberg MD, and Walls AF (2004). Inhibitors of tryptase as mast cell-stabilizing agents in the human airways: effects of tryptase and other agonists of proteinase-activated receptor 2 on histamine release. J Pharmacol Exp Ther 309, 119–126. [PubMed: 14722328]

He S, and Walls AF (1997). Human mast cell tryptase: a stimulus of microvascular leakage and mast cell activation. European journal of pharmacology 328, 89–97. [PubMed: 9203574]

Huang C, Li L, Krilis SA, Chanasyk K, Tang Y, Li Z, Hunt JE, and Stevens RL (1999). Human tryptases alpha and beta/II are functionally distinct due, in part, to a single amino acid difference in one of the surface loops that forms the substrate-binding cleft. The Journal of biological chemistry 274, 19670–19676. [PubMed: 10391906]

Huber R, and Bode W (1978). Structural basis of the activation and action of trypsin. Acc Chem Res 11, 114–122.

Iddamalgoda A, Le QT, Ito K, Tanaka K, Kojima H, and Kido H (2008). Mast cell tryptase and photoaging: possible involvement in the degradation of extra cellular matrix and basement membrane proteins. Arch Dermatol Res 300 Suppl 1, S69–76. [PubMed: 17968569]

Iwashita K, Kawasaki H, Sawada M, In M, Mataki Y, and Kuwabara T (2008). Shortening of the induction period of allergic asthma in cynomolgus monkeys by Ascaris suum and house dust mite. J Pharmacol Sci 106, 92–99. [PubMed: 18187925]

Jia G, Erickson RW, Choy DF, Mosesova S, Wu LC, Solberg OD, Shikotra A, Carter R, Audusseau S, Hamid Q, et al. (2012). Periostin is a systemic biomarker of eosinophilic airway inflammation in asthmatic patients. J Allergy Clin Immunol 130, 647–654 e610. [PubMed: 22857879]

Jogie-Brahim S, Min HK, Fukuoka Y, Xia HZ, and Schwartz LB (2004). Expression of alpha-tryptase and beta-tryptase by human basophils. The Journal of allergy and clinical immunology 113, 1086–1092. [PubMed: 15208589]

Kan ZY, Walters BT, Mayne L, and Englander SW (2013). Protein hydrogen exchange at residue resolution by proteolytic fragmentation mass spectrometry analysis. Proc Natl Acad Sci USA 110, 16438–16443. [PubMed: 24019478]

Kaur D, Saunders R, Hollins F, Woodman L, Doe C, Siddiqui S, Bradding P, and Brightling C (2010). Mast cell fibroblastoid differentiation mediated by airway smooth muscle in asthma. J Immunol 185, 6105–6114. [PubMed: 20952685]

Krishna MT, Chauhan A, Little L, Sampson K, Hawksworth R, Mant T, Djukanovic R, Lee T, and Holgate S (2001). Inhibition of mast cell tryptase by inhaled APC 366 attenuates allergen-induced late-phase airway obstruction in asthma. J Allergy Clin Immunol 107, 1039–1045. [PubMed: 11398082]

Lawrence MC, and Colman PM (1993). Shape complementarity at protein/protein interfaces. Journal of molecular biology 234, 946–950. [PubMed: 8263940]

Le QT, Lyons JJ, Naranjo AN, Olivera A, Lazarus RA, Metcalfe DD, Milner JD, and Schwartz LB (2019). Impact of naturally forming human alpha/beta-tryptase heterotetramers in the pathogenesis of hereditary alpha-tryptasemia. J Exp Med. [Epub ahead of print]

Liang G, Aldous S, Merriman G, Levell J, Pribish J, Cairns J, Chen X, Maignan S, Mathieu M, Tsay J, et al. (2012). Structure-based library design and the discovery of a potent and selective mast cell beta-tryptase inhibitor as an oral therapeutic agent. Bioorganic & medicinal chemistry letters 22, 1049–1054. [PubMed: 22192588]

Lyons JJ, Stotz SC, Chovanec J, Liu Y, Lewis KL, Nelson C, DiMaggio T, Jones N, Stone KD, Sung H, et al. (2018). A common haplotype containing functional CACNA1H variants is frequently coinherited with increased TPSAB1 copy number. Genet Med 20, 503–512. [PubMed: 28933792]

Lyons JJ, Yu X, Hughes JD, Le QT, Jamil A, Bai Y, Ho N, Zhao M, Liu Y, O'Connell MP, et al. (2016). Elevated basal serum tryptase identifies a multisystem disorder associated with increased TPSAB1 copy number. Nat Genet 48, 1564–1569. [PubMed: 27749843]

Macaraeg NF, Reilly DE, and Wong AW (2013). Use of an anti-apoptotic CHO cell line for transient gene expression. Biotechnol Prog 29, 1050–1058. [PubMed: 23794499]

Maddox L, and Schwartz DA (2002). The pathophysiology of asthma. Annu Rev Med 53, 477–498. [PubMed: 11818486]

Maun HR, Liu PS, Franke Y, Eigenbrot C, Forrest WF, Schwartz LB, and Lazarus RA (2018). Dual functionality of beta-tryptase protomers as both proteases and cofactors in the active tetramer. The Journal of biological chemistry 293, 9614–9628. [PubMed: 29661938]

Mayne L, Kan ZY, Chetty PS, Ricciuti A, Walters BT, and Englander SW (2011). Many overlapping peptides for protein hydrogen exchange experiments by the fragment separation-mass spectrometry method. Journal of the American Society for Mass Spectrometry 22, 1898–1905. [PubMed: 21952777]

McCoy AJ, Grosse-Kunstleve RW, Adams PD, Winn MD, Storoni LC, and Read RJ (2007). Phaser crystallographic software. Journal of applied crystallography 40, 658–674. [PubMed: 19461840]

Murshudov GN, Skubak P, Lebedev AA, Pannu NS, Steiner RA, Nicholls RA, Winn MD, Long F, and Vagin AA (2011). REFMAC5 for the refinement of macromolecular crystal structures. Acta Crystallogr D Biol Crystallogr 67, 355–367. [PubMed: 21460454]

Ortega HG, Liu MC, Pavord ID, Brusselle GG, FitzGerald JM, Chetta A, Humbert M, Katz LE, Keene ON, Yancey SW, et al. (2014). Mepolizumab treatment in patients with severe eosinophilic asthma. N Engl J Med 371, 1198–1207. [PubMed: 25199059]

Ortega HG, Yancey SW, Mayer B, Gunsoy NB, Keene ON, Bleecker ER, Brightling CE, and Pavord ID (2016). Severe eosinophilic asthma treated with mepolizumab stratified by baseline eosinophil thresholds: a secondary analysis of the DREAM and MENSA studies. Lancet Respir Med 4, 549–556. [PubMed: 27177493]

Otwinowski Z, M. W (1997). Processing of X-ray diffraction data collected in oscillation mode. Methods in Enzymol 276, 307–326.

Paganin F, Mangiapan G, Proust A, Prudhomme A, Attia J, Marchand-Adam S, Pellet F, Milhe F, Melloni B, Bernady A, et al. (2017). Lung function parameters in omalizumab responder patients: An interesting tool? Allergy 72, 1953–1961. [PubMed: 28517027]

Page S, Ammit AJ, Black JL, and Armour CL (2001). Human mast cell and airway smooth muscle cell interactions: implications for asthma. Am J Physiol Lung Cell Mol Physiol 281, L1313–1323. [PubMed: 11704524]

Pallaoro M, Fejzo MS, Shayesteh L, Blount JL, and Caughey GH (1999). Characterization of genes encoding known and novel human mast cell tryptases on chromosome 16p13.3. The Journal of biological chemistry 274, 3355–3362. [PubMed: 9920877]

Pan Z, Jeffery DA, Chehade K, Beltman J, Clark JM, Grothaus P, Bogyo M, and Baruch A (2006). Development of activity-based probes for trypsin-family serine proteases. Bioorganic & medicinal chemistry letters 16, 2882–2885. [PubMed: 16554154]

Pereira PJ, Bergner A, Macedo-Ribeiro S, Huber R, Matschiner G, Fritz H, Sommerhoff CP, and Bode W (1998). Human β-tryptase is a ring-like tetramer with active sites facing a central pore. Nature 392, 306–311. [PubMed: 9521329]

Rabe KF, Nair P, Brusselle G, Maspero JF, Castro M, Sher L, Zhu H, Hamilton JD, Swanson BN, Khan A, et al. (2018). Efficacy and Safety of Dupilumab in Glucocorticoid-Dependent Severe Asthma. N Engl J Med 378, 2475–2485. [PubMed: 29782224]

Ray A, Raundhal M, Oriss TB, Ray P, and Wenzel SE (2016). Current concepts of severe asthma. J Clin Invest 126, 2394–2403. [PubMed: 27367183]

Ren S, Lawson AE, Carr M, Baumgarten CM, and Schwartz LB (1997). Human tryptase fibrinogenolysis is optimal at acidic pH and generates anticoagulant fragments in the presence of the anti-tryptase monoclonal antibody B12. J Immunol 159, 3540–3548. [PubMed: 9317153]

Schwartz LB, and Bradford TR (1986). Regulation of tryptase from human lung mast cells by heparin. Stabilization of the active tetramer. The Journal of biological chemistry 261, 7372–7379. [PubMed: 3519608]

Schwartz LB, Bradford TR, Lee DC, and Chlebowski JF (1990). Immunologic and physicochemical evidence for conformational changes occurring on conversion of human mast cell tryptase from active tetramer to inactive monomer. Production of monoclonal antibodies recognizing active tryptase. Journal of immunology (Baltimore, Md : 1950) 144, 2304–2311.

Schwartz LB, Bradford TR, Littman BH, and Wintroub BU (1985). The fibrinogenolytic activity of purified tryptase from human lung mast cells. Journal of immunology (Baltimore, Md : 1950) 135, 2762–2767.

Schwartz LB, Lewis RA, and Austen KF (1981). Tryptase from human pulmonary mast cells. Purification and characterization. The Journal of biological chemistry 256, 11939–11943. [PubMed: 7028744]

Sekizawa K, Caughey GH, Lazarus SC, Gold WM, and Nadel JA (1989). Mast cell tryptase causes airway smooth muscle hyperresponsiveness in dogs. J Clin Invest 83, 175–179. [PubMed: 2642918]

Siddiqui S, Shikotra A, Richardson M, Doran E, Choy D, Bell A, Austin CD, Eastham-Anderson J, Hargadon B, Arron JR, et al. (2018). Airway pathological heterogeneity in asthma: Visualization of disease microclusters using topological data analysis. The Journal of allergy and clinical immunology 142, 1457–1468. [PubMed: 29550052]

Simpson LJ, Patel S, Bhakta NR, Choy DF, Brightbill HD, Ren X, Wang Y, Pua HH, Baumjohann D, Montoya MM, et al. (2014). A microRNA upregulated in asthma airway T cells promotes TH2 cytokine production. Nat Immunol 15, 1162–1170. [PubMed: 25362490]

Sommerhoff CP, Bode W, Pereira PJ, Stubbs MT, Sturzebecher J, Piechottka GP, Matschiner G, and Bergner A (1999). The structure of the human βII-tryptase tetramer: Fo(u)r better or worse. Proc Natl Acad Sci USA 96, 10984–10991. [PubMed: 10500112]

Song HK, and Suh SW (1998). Kunitz-type soybean trypsin inhibitor revisited: refined structure of its complex with porcine trypsin reveals an insight into the interaction between a homologous inhibitor from Erythrina caffra and tissue-type plasminogen activator. Journal of molecular biology 275, 347–363. [PubMed: 9466914]

Staton TL, Choy DF, and Arron JR (2016). Biomarkers in the clinical development of asthma therapies. Biomark Med 10, 165–176. [PubMed: 26764286]

Sutcliffe A, Kaur D, Page S, Woodman L, Armour CL, Baraket M, Bradding P, Hughes JM, and Brightling CE (2006). Mast cell migration to Th2 stimulated airway smooth muscle from asthmatics. Thorax 61, 657–662. [PubMed: 16601090]

Sutton JC, Bolton SA, Hartl KS, Huang MH, Jacobs G, Meng W, Ogletree ML, Pi Z, Schumacher WA, Seiler SM, et al. (2002). Synthesis and SAR of 4-carboxy-2-azetidinone mechanism-based tryptase inhibitors. Bioorganic & medicinal chemistry letters 12, 3229–3233. [PubMed: 12372540]

Tam EK, and Caughey GH (1990). Degradation of airway neuropeptides by human lung tryptase. American journal of respiratory cell and molecular biology 3, 27–32. [PubMed: 1694672]

Trivedi NN, and Caughey GH (2010). Mast cell peptidases: chameleons of innate immunity and host defense. American journal of respiratory cell and molecular biology 42, 257–267. [PubMed: 19933375]

Trivedi NN, Tamraz B, Chu C, Kwok PY, and Caughey GH (2009). Human subjects are protected from mast cell tryptase deficiency despite frequent inheritance of loss-of-function mutations. The Journal of allergy and clinical immunology 124, 1099–1105 e1091–1094. [PubMed: 19748655]

Walters BT, Mayne L, Hinshaw JR, Sosnick TR, and Englander SW (2013). Folding of a large protein at high structural resolution. Proc Natl Acad Sci USA 110, 18898–18903. [PubMed: 24191053]

Walters BT, Ricciuti A, Mayne L, and Englander SW (2012). Minimizing back exchange in the hydrogen exchange-mass spectrometry experiment. Journal of the American Society for Mass Spectrometry 23, 2132–2139. [PubMed: 22965280]

Winn MD, Ballard CC, Cowtan KD, Dodson EJ, Emsley P, Evans PR, Keegan RM, Krissinel EB, Leslie AG, McCoy A, et al. (2011). Overview of the CCP4 suite and current developments. Acta Crystallogr D Biol Crystallogr 67, 235–242. [PubMed: 21460441]

Woodman L, Siddiqui S, Cruse G, Sutcliffe A, Saunders R, Kaur D, Bradding P, and Brightling C (2008). Mast cells promote airway smooth muscle cell differentiation via autocrine up-regulation of TGF-beta 1. J Immunol 181, 5001–5007. [PubMed: 18802103]

Woodruff PG, Modrek B, Choy DF, Jia G, Abbas AR, Ellwanger A, Koth LL, Arron JR, and Fahy JV (2009). T-helper type 2-driven inflammation defines major subphenotypes of asthma. Am J Respir Crit Care Med 180, 388–395. [PubMed: 19483109]

Wright CD, Havill AM, Middleton SC, Kashem MA, Dripps DJ, Abraham WM, Thomson DS, and Burgess LE (1999). Inhibition of allergen-induced pulmonary responses by the selective tryptase inhibitor 1,5-bis-[4-[(3-carbamimidoyl-benzenesulfonylamino)-methyl]-phenoxy]-pen tane (AMG-126737). Biochem Pharmacol 58, 1989–1996. [PubMed: 10591155]

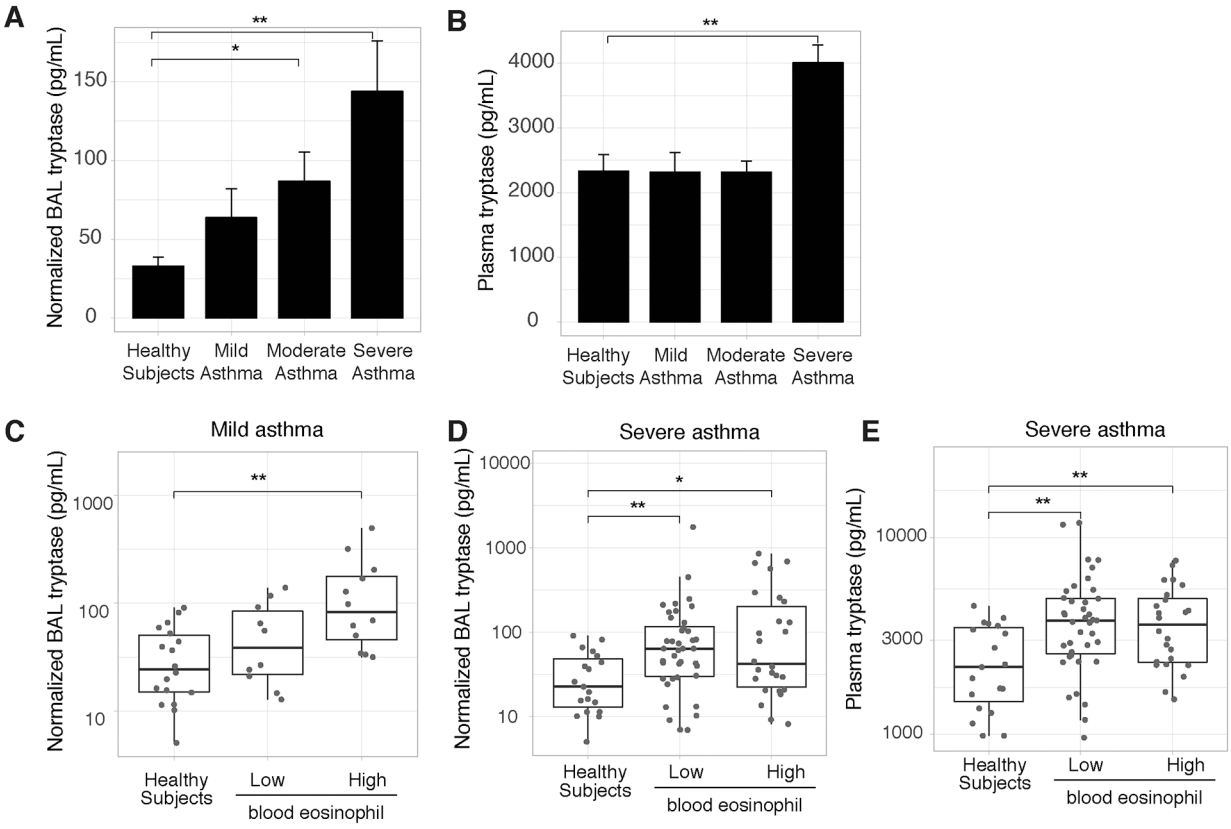

Figure 1. Elevated total tryptase in severe asthma patients independent of type 2 inflammation.

(**A**, **B**) Tryptase in BAL fluid (**A**) and plasma (**B**). Albumin-normalized BAL tryptase levels (mean ± SE) to account for dilution. Patient numbers are in methods. (**C**) Normalized tryptase in BAL fluid of mild asthma patients stratified by blood eosinophil counts (300 cells/μL as cutoff). (**D, E**) Tryptase in BAL fluid or plasma of healthy subjects and severe asthma patients stratified as in (**C**). Each dot is an individual patient. Mann-Whitney tests were used to compare differences between groups *p<0.05, **p<0.01, ***p<0.001.

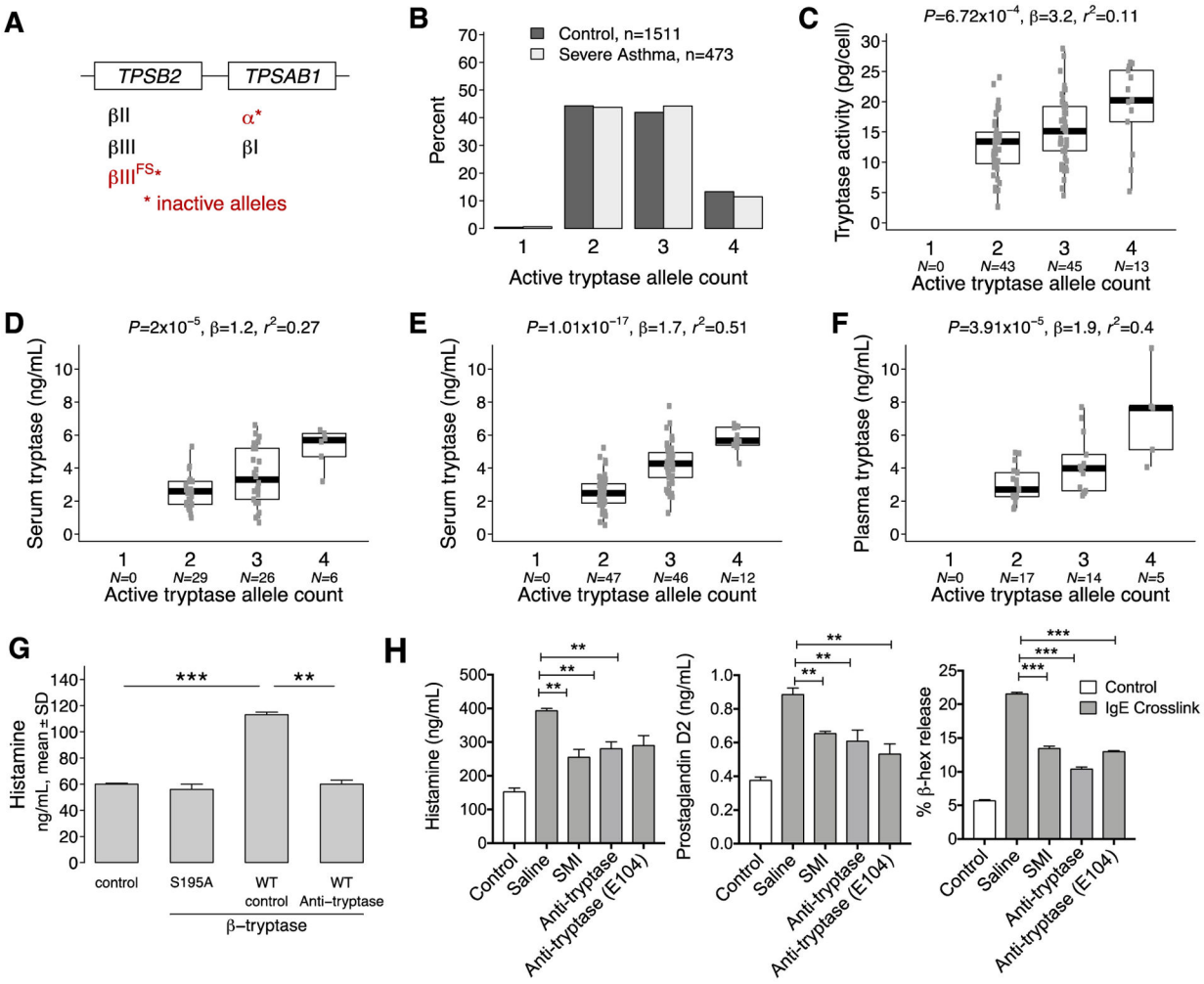

Figure 2. Active tryptase allele count is correlated with systemic tryptase levels.

(A) Schematic diagram of tryptase gene loci. (**B**) Percentage of healthy controls and asthma patients with 1, 2, 3, or 4 active tryptase allele count. (**C**) The level of tryptase activity per primary MC from foreskins of human donors (*N*=101) was assessed *ex vivo* with respect to active tryptase allele count. (**D**) Serum tryptase levels in healthy subjects with different active tryptase allele count. Serum (**E**) and plasma (**F**) tryptase levels from severe uncontrolled asthma subjects with different active tryptase allele count. *P*-value, correlation estimate (β), and r^2 from linear regression are annotated on plots. (**G**) Histamine concentrations in culture supernatants in LAD2 cells degranulated by inactive β-tryptase (S195A), wild-type (WT) β-tryptase, or β-tryptase + anti-tryptase. (**H**) Histamine, prostaglandin D2 (PGD2) and percentage of total β-hexosaminidase release in culture supernatant of LAD2 cells treated with saline or IgE/anti-IgE immune complex with or without indicated tryptase SMI or two different clones of inhibitory anti-tryptase IgG antibodies (31A.v11 or E104); mean ± SD (n=3).

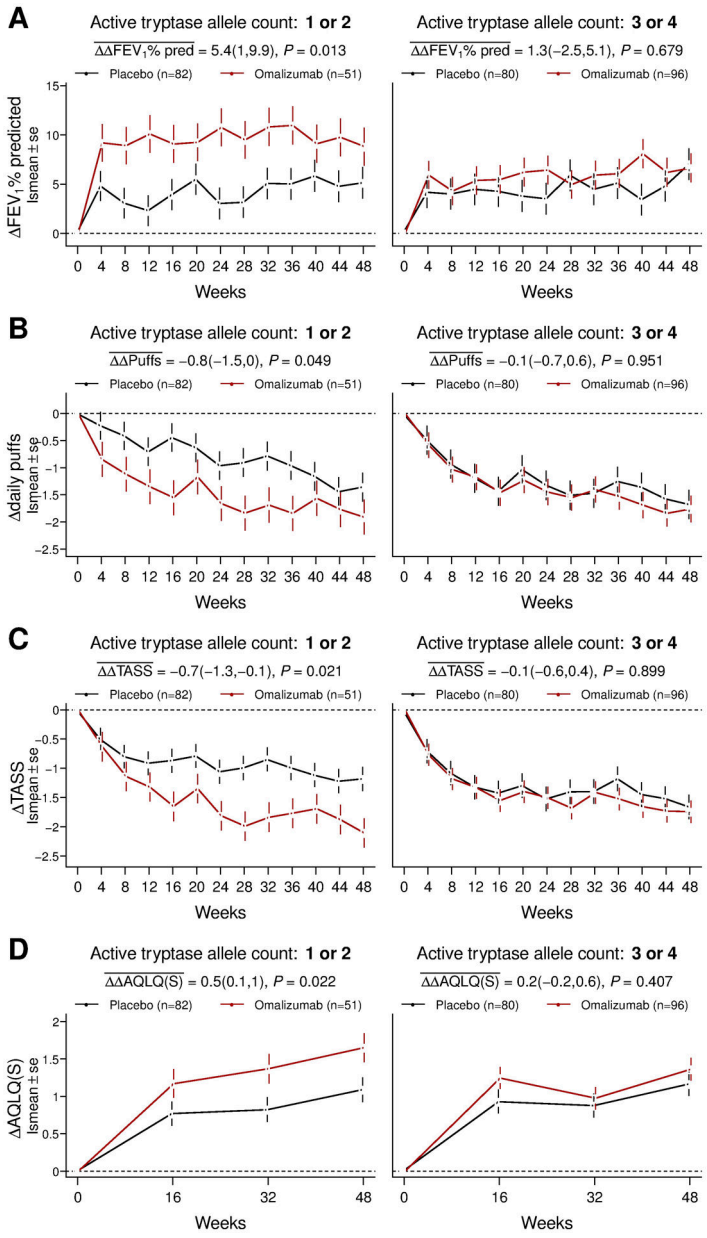

Figure 3. Treatment benefit from anti-IgE therapy in asthma patients based on active tryptase copy number

(**A**) FEV_1 percent. (**B**) Daily number of puffs of albuterol change. (**C**) Total asthma symptom severity scores (TASS). (**D**) Overall asthma quality of life with standardized activities (AQLQ[S]). Changes from baseline were assessed in patients from the EXTRA study on the basis of active tryptase copy number (1 or 2 left, 3 or 4 right). Least squares (mean ± SE) are plotted and the mean post-treatment placebo controlled treatment effect estimated by linear contrast are annotated in the plot margins.

A

Biacore analysis of kinetic parameters for antigen binding to anti-tryptase

	k_{ON} ($10^5 M^{-1}s^{-1}$)	k_{OFF} ($10^{-4}s^{-1}$)	K_D (nM)
α-tryptase	6.7 ± 0.2	2.4 ± 0.6	0.36 ± 0.08
βI-tryptase	6.4 ± 0.7	1.6 ± 0.3	0.25 ± 0.02
βII-tryptase	14.0 ± 0.6	1.5 ± 0.1	0.11 ± 0.02
βIII-tryptase	15.0 ± 0.8	1.3 ± 0.2	0.09 ± 0.01

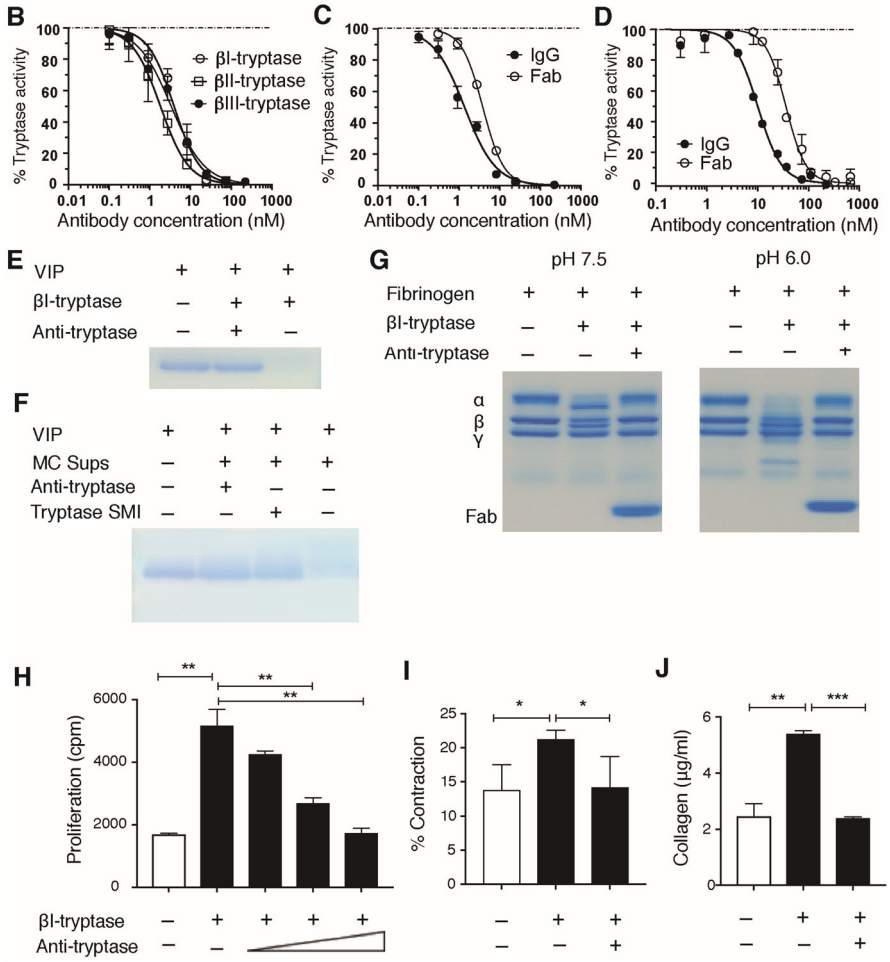

Figure 4. Identification of a high affinity inhibitory anti-tryptase IgG4 antibody.

(**A**) Binding kinetics of anti-tryptase to human tryptase. (**B, C**) Tryptase activity using S-2288 peptide substrate for βI-, βII-, βIII-tryptases with anti-tryptase (**B**) and for βI-tryptase with anti-tryptase Fab or IgG4 antibody (**C**). (**D**) Tryptase activity using ES002 peptide substrate with degranulated foreskin MC releasate with anti-tryptase Fab or IgG4. (**E, F**) VIP peptide degradation by βI-tryptase (**E**) or degranulated MC supernatant (**F**) with saline control, anti-tryptase, or a tryptase small molecule inhibitor (SMI). (**G**) Fibrinogen α chain degradation by βI-tryptase with or without anti-tryptase at pH 7.5 or pH 6.0. (**H**) Primary human SMC proliferation stimulated by βI-tryptase with or without anti-tryptase. (**I**) Primary human SMC contraction induced by βI-tryptase with or without anti-tryptase. (**J**) Collagen secretion by primary human lung fibroblasts induced by recombinant βI-

tryptase treated with anti-tryptase or medium. Data for A-D and H-J are mean ± SE (n=3); student's t-test was used to compare between two groups. *p<0.05, **p<0.01, ***p<0.001.

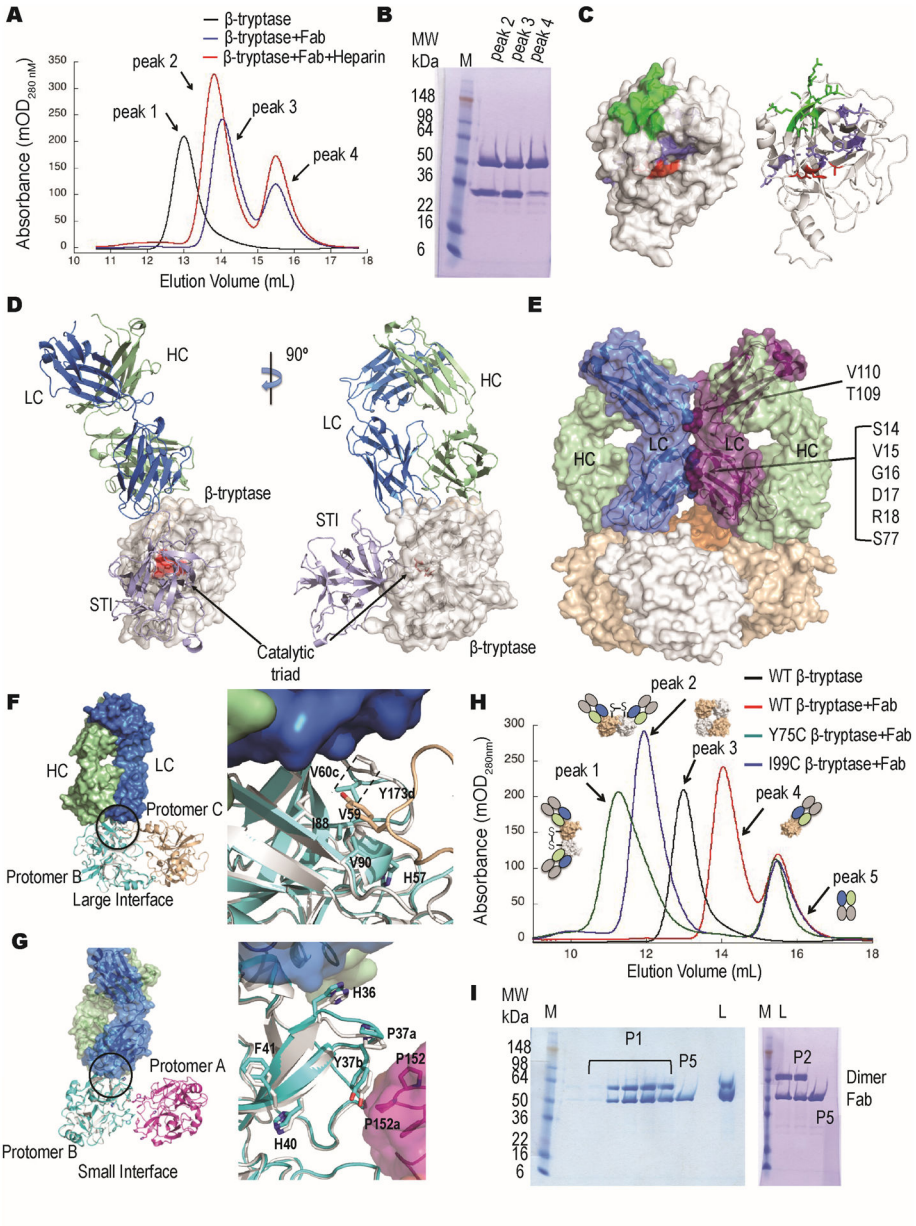

Figure 5. A crystal structure reveals an allosteric mode of anti-tryptase binding and a tetramer dissociation mechanism.

(**A**) SEC of anti-tryptase Fab (31A.v11) in complex with βI-tryptase with or without heparin. Tetrameric βI-tryptase alone (Peak 1, black) and Fab (Peak 4, blue and red) eluted at 13.0 mL and 15.5 mL, respectively. A complex of tetrameric βI-tryptase incubated with excess Fab in the presence (Peak 2, red) or absence (Peak 3, blue) of 0.1 mg/mL heparin eluted at 13.8 mL and 14.05 mL, respectively. (**B**) Non-reducing SDS-PAGE of peak fractions. (**C**) Depictions in surface (left) and cartoon (right) of slower H-D exchange areas in green (large surface cluster) and slate when Fab is bound to βI-tryptase; catalytic triad residues are in red. (**D**) Crystal structure of βI-tryptase monomer (white) bound to anti-tryptase Fab (31A.v11) and soybean trypsin inhibitor (STI, in slate) determined at 2.15 Å resolution; HC and LC are in green and blue, respectively. Catalytic triad residues are

in red. (**E**) The βI-tryptase monomer in complex with anti-tryptase was superposed with protomers A and C (beige) of the β-tryptase tetramer (1A0L); protomers B and D in the tetramer are white and orange. Residue clashes between the LCs (blue and purple) of the Fab are labeled and shown as spheres; identical residues in each LC clash with each other. (**F**, **G**) Conformational changes in the 60s (**F**) and 30s (**G**) loop of βI-tryptase upon Fab binding that affect the large (Protomers B and C in white and beige) or small (Protomers B and A in white and magenta) interface, respectively. (Left panels) βI-tryptase (cyan) from the Fab complex was superposed with Protomer B (white) from the tetramer (1A0L). Right panels show closeup interface views in the circle. Key interface residues and catalytic triad residue H57 are shown in sticks (**F**). (**H**, **I**) SEC of anti-tryptase Fab in complex with WT and two different disulfide-locked variants (Y75C and I99C) of tetrameric βI-tryptase. Tetrameric βI-tryptase alone (Peak 3, black) and Fab (Peak 5, red, blue and green) had elution volumes (V_e) of 13.0 mL and 15.5 mL, respectively. Complexes of tetrameric βI-tryptase incubated with excess Fab for WT (Peak 4, red), Y75C (Peak 1, green) and I99C (Peak 2, blue) eluted at 14.0 mL (Monomer/Fab), 11.3 mL (Dimer/2 Fabs) and 11.9 mL (Dimer/2Fabs), respectively. Non-reducing SDS-PAGE of peak fractions for Y75C βI-tryptase and Fab (**I**, left panel) and I99C βI-tryptase and Fab (**I**, right panel) are shown. Dimer refers to βI-tryptases Y75C (**I**, left panel) and I99C (**I**, right panel). M, L, P1, P2 and P5 refer to Markers, Load, Peak 1, Peak 2 and Peak 5, respectively.

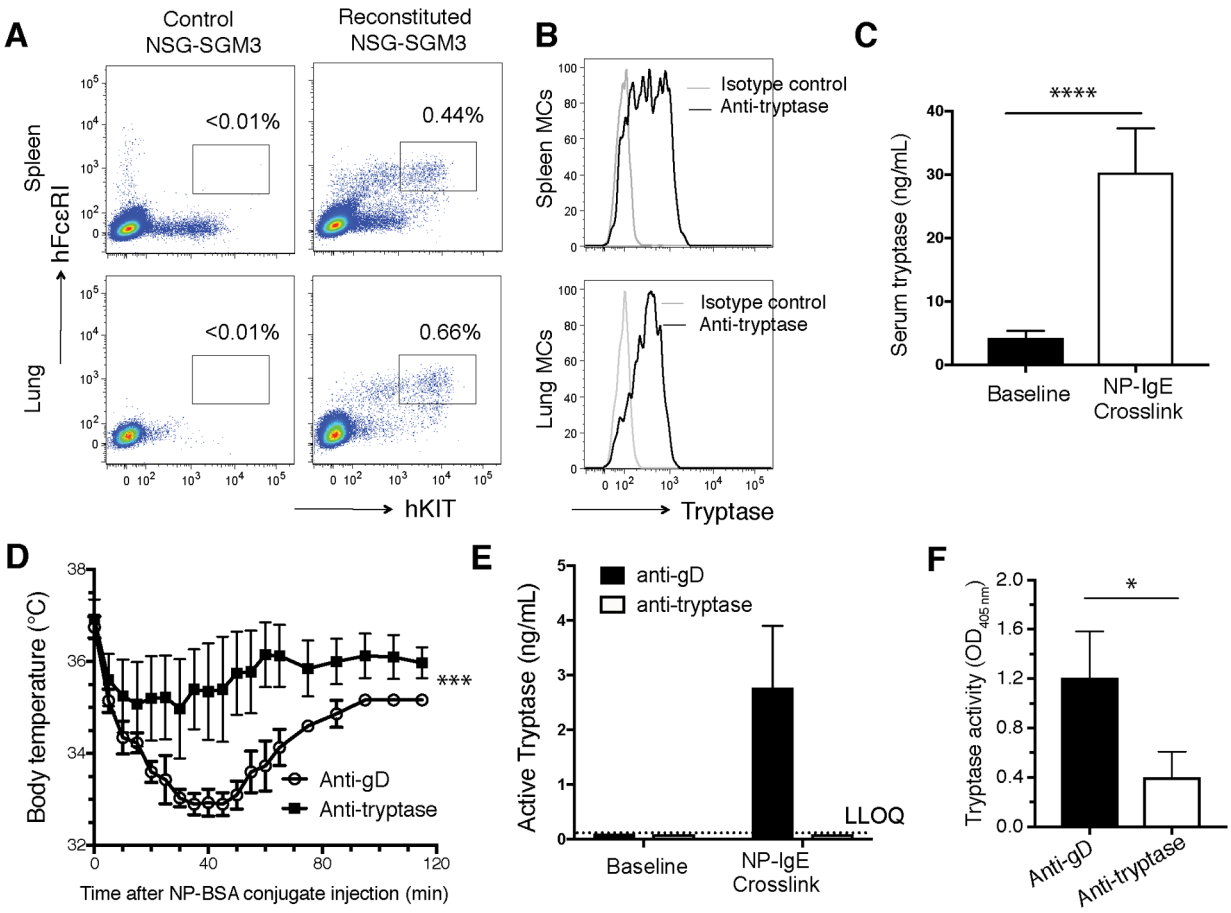

Figure 6. Anti-tryptase antibody inhibits tryptase activity *in vivo* and attenuates MC-induced anaphylaxis response.

(**A, B**) FACS analysis of human MCs (defined as $KIT^+Fc\varepsilon RI^+$) cells in spleen and lung of control NOD.*scid*.SGM3 mice or NOD.*scid*.SGM3 mice reconstituted with human $CD34^+$ stem cells (**A**). Intracellular tryptase staining in MCs from spleen and lung (**B**). (**C**, **D**) NOD.*scid*.SGM3 animals reconstituted human $CD34^+$ stem cells were injected with anti-NP IgE and NP-BSA conjugates. (**C**) Total tryptase concentration after anti-NP IgE and NP-BSA conjugates crosslinking; mean ± SE (n=4). (**D**) Anti-tryptase or anti-gD (isotype control) injected 24 h before the anti-IgE administration. Body temperature measurement after NP-BSA conjugate injection. mean ± SE (n=4). (**E**) Active tryptase concentration in BAL in humanized mice at baseline or 10 min after anti-NP IgE/NP-BSA crosslinking; mean ± SE (n=4). Lower limit of quantification (LLOQ) is 0.3 ng/mL. (**F**) Tryptase enzymatic activity measured with S-2288 substrate in the presence of α1-antitrypsin and STI in BAL fluid 10 min after NP-BSA conjugate injection; mean ± SE (n=3) *$p<0.05$, ***$p<0.001$.

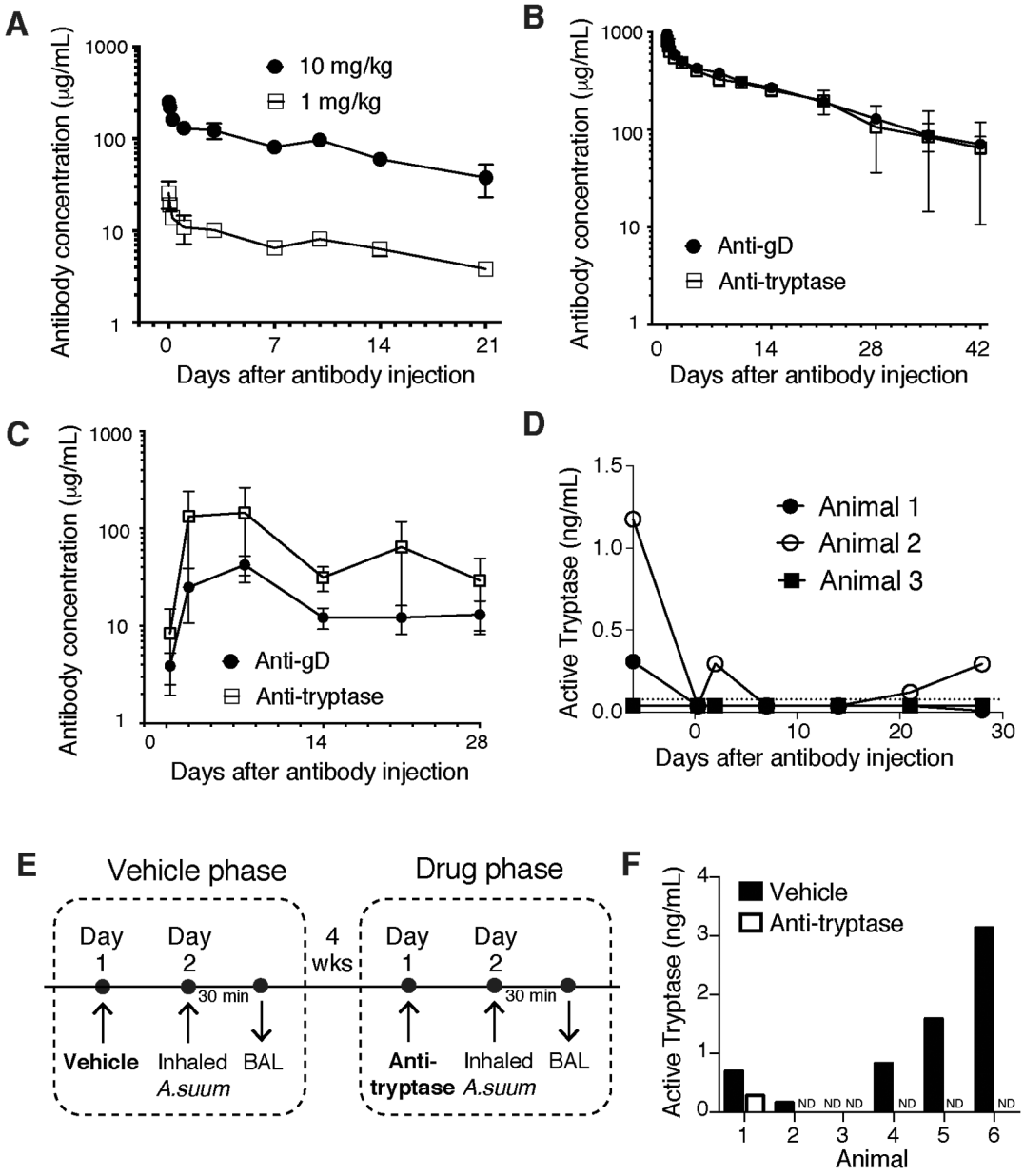

Figure 7. Anti-tryptase IgG4 antibody exhibits favorable pharmacokinetics and reduces tryptase activity in BAL in nonhuman primates.

(**A**) Antibody concentration in NOD.*scid* mice dosed IV with anti-tryptase IgG4 antibody. (**B, C**) Antibody concentration in blood (**B**) or BAL fluid (**C**) of cynomolgus monkey injected SC with a single dose (30 mg/kg) of anti-tryptase or anti-gD human IgG4. **(D)** Tryptase activity quantified by an activity-based probe assay in BAL fluid of cynomolgus monkeys on study days -6, 1 (8 h post-dose), 3, 8, 15, 22, and 29. The dotted line is the lower limit of quantification. **(E)** Study schema for treatment and sampling of sensitized cynomolgus monkeys after inhaled challenge with *Ascaris suum*. Each animal underwent a vehicle and drug treatment phase, thereby serving as its own control. **(F)** Tryptase activity quantified using an activity-based probe assay in BAL fluid of *Ascaris suum* sensitized

cynomolgus monkeys after inhaled *Ascaris suum* challenge. “ND” denotes samples below the lower limit of detection. $p<0.05$, paired Student’s t-test.